

**AIR COUPLED IMPACT ECHO TESTING OF BURIED  
CONCRETE PIPES**

by

Yash Kumar Dhabi, B.Tech., M.Tech

A Thesis Presented in Partial Fulfillment  
of the Requirements of the Degree  
Doctor of Philosophy

COLLEGE OF ENGINEERING AND SCIENCE  
LOUISIANA TECH UNIVERSITY

May 2023

LOUISIANA TECH UNIVERSITY

GRADUATE SCHOOL

April 18, 2023

Date of dissertation defense

We hereby recommend that the dissertation prepared by

**Yash Kumar Dhabi, B.Tech, M.Tech.**

entitled **Air Coupled Impact Echo Testing of Buried Concrete Pipes**

be accepted in partial fulfillment of the requirements for the degree of

**Doctor of Philosophy in Engineering, Micro & Nanoscale Systems Conc.**



Dr. Arun Jaganathan  
Supervisor of Dissertation Research

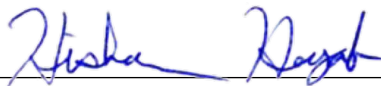


Dr. Shengnian Wang  
Head of Engineering

**Doctoral Committee Members:**

Dr. Neven Simicevic  
Dr. John Matthews  
Dr. Leland Weiss  
Dr. Jay Xingran Wang

**Approved:**



Hisham Hegab  
Dean of Engineering & Science

**Approved:**



Ramu Ramachandran  
Dean of the Graduate School

## **ABSTRACT**

Concrete pipes constitute an integral part of the buried infrastructure, and non-destructive testing (NDT) plays an important role in their maintenance effort. Impact echo (IE) is a well-established NDT technique that is widely used for the investigation of concrete structures. In this technique, the thickness (or resonant) frequency is first measured by inducing (compression) P-wave into the structure using an impact source and recording the elastic wave generated using an accelerometer. From the knowledge of P-wave velocity of the medium, the unknown thickness and subsurface defects are then established. To effectively apply this technique, the transducer should be properly coupled with the surface. However, this often becomes a difficult task due to the poor surface quality of concrete. Alternatively, instead of capturing the elastic wave with a contact-based transducer the leaky acoustic wave that accompany the elastic wave is captured with a microphone and the thickness frequency is calculated. This non-contact variation of IE is called the air-coupled IE (ACIE) and it has been shown to be effective for testing plate like concrete structures (e.g., pavements and bridge decks). In this dissertation, the feasibility of ACIE for the NDT of buried concrete pipe is investigated. The investigations are conducted in two stages. First, numerical modelling is conducted to test the effectiveness in pipes and then experimental validations are conducted. A structural-acoustic coupled finite element model is created using the COMSOL Multiphysics software, and the propagation of elastic and acoustic waves in a fluid-filled

concrete pipe is simulated for standalone and buried pipe. The effectiveness of ACIE is studied when a pipe is surrounded by soil. Two types of soil surrounding the pipe studied to learn more about the quality of the data that might be anticipated from ACIE technique inside the pipe. Using these models, various aspects of ACIE are studied and its performance against the conventional IE is compared. Following the numerical verifications, two laboratory tests setups are constructed with a standalone and buried reinforced concrete pipes (RCP) and ACIE is demonstrated using them. The (unknown) wall thickness is calculated in each case and the results are compared against the conventional contact-based technique. While the presence of soil caused energy losses which affected the amplitude of acoustic wave, it was enough to be detected with good signal to noise ratio.

Several enhancements to improve the performance of this technique are studied. For instance, a way to improve the signal-to noise ratio of the acoustic signal is investigated using noise suppressers. For rapid implementation of technique and fast data gathering a semi-automated ACIE setup is also developed. Finally, the ability of the technique to detect several commonly occurring problems in a concrete pipe is investigated.

In summary, ACIE technique shows promising results for buried pipe testing.

## **APPROVAL FOR SCHOLARLY DISSEMINATION**

The author grants to the Prescott Memorial Library of Louisiana Tech University the right to reproduce, by appropriate methods, upon request, any or all portions of this Thesis. It is understood that “proper request” consists of the agreement, on the part of the requesting party, that said reproduction is for his personal use and that subsequent reproduction will not occur without written approval of the author of this Thesis. Further, any portions of the Thesis used in books, papers, and other works must be appropriately referenced to this Thesis.

Finally, the author of this Thesis reserves the right to publish freely, in the literature, at any time, any or all portions of this Thesis.

Author \_\_\_\_\_

Date \_\_\_\_\_

## **DEDICATION**

This Dissertation is dedicated to my beloved grandfather, Sh. Jaganath Dhabhi; to my beloved parents, Sh. Partap Singh Dhabhi (father) and Smt. Kiran Devi (Mother); to all my family members, friends and my advisors who have made the completion of this dissertation possible.

## TABLE OF CONTENTS

ABSTRACT.....	iii
APPROVAL FOR SCHOLARLY DISSEMINATION .....	v
DEDICATION .....	vi
LIST OF FIGURES .....	x
LIST OF TABLES .....	xiii
ACKNOWLEDGMENTS .....	xiv
CHAPTER 1 INTRODUCTION .....	1
1.1 Background and motivation.....	1
1.2 Objectives .....	4
1.3 Dissertation outline.....	4
CHAPTER 2 IMPACT ECHO AND AIR COUPLED IMPACT ECHO: AN OVERVIEW .....	6
2.1 Instrumentation .....	9
2.1.1 Impactor .....	10
2.1.2 Transducer.....	10
2.1.3 Contact transducer .....	10
2.1.4 Non-contact transducer .....	11
2.1.5 Data acquisition system (DAQ) .....	11
CHAPTER 3 NUMERICAL MODELLING OF AIR COUPLED IMPACT ECHO .....	12
3.1 Introduction.....	12
3.2 Governing equations .....	13

3.2.1	Elastic domain:.....	13
3.2.2	Acoustic domain .....	14
3.2.3	Interface between acoustic and elastic domains: .....	15
3.3	Impact .....	15
3.4	Computational mesh size and time steps .....	17
3.5	Model 1: 2D model with a standalone pipe .....	18
3.6	Model 2: 3D model with a standalone pipe .....	20
3.7	Model 3: 2D model with a buried pipe .....	21
3.7.1	Soil properties .....	22
3.8	Results and discussion .....	24
3.8.1	Model 1 & Model 2.....	24
3.8.2	Parametric study.....	28
3.8.3	Model 3 .....	29
3.9	Conclusions.....	32
<b>CHAPTER 4 AIR-COUPLED IMPACT ECHO TESTING OF BURIED REINFORCED CONCRETE PIPES:</b> .....		<b>34</b>
<b>AN EXPERIMENTALSTUDY</b> .....		<b>34</b>
4.1	Introduction.....	34
4.2	ACIE testing of standalone pipe segment.....	34
4.2.1	Instrumentation .....	34
4.2.2	Comparison of ACIE and IE results .....	37
4.2.3	Parametric study- microphone placement.....	39
4.2.4	Characterization of entire pipe.....	40
4.2.5	Design of noise suppressor .....	42
4.2.6	Buried concrete pipe .....	44
4.2.7	Result and discussion.....	46



4.3	Conclusions.....	48
CHAPTER 5 A SEMI AUTOMATED AIR COUPLED INVESTIGATION OF CONCRETE PIPE .....		50
5.1	Introduction.....	50
5.1.1	Semi-automated ACIE setup.....	50
5.1.2	Input waveform.....	51
5.1.3	Experimental setup.....	52
5.1.4	Comparison between condenser and MEMS microphone.....	53
5.2	Noise reduction study .....	54
5.3	Conclusions.....	55
CHAPTER 6 INVESTIGATION OF PIPEWALL DEFECTS USING ACIE.....		57
6.1	Introduction.....	57
6.2	Common flaws in concrete pipe. ....	57
6.2.1	Thickness loss .....	57
6.2.2	Delamination.....	58
6.2.3	Soil voids .....	59
6.3	Numerical modeling of pipe wall defects.....	59
6.4	Results and discussion .....	61
6.4.1	Model 1: Effect of thickness loss.....	61
6.4.2	Model 2: Effect of delamination.....	62
6.4.3	Model 3: Effect of soil void.....	64
6.5	Conclusions.....	65
CHAPTER 7 CONCLUSION.....		66
7.1	Future work.....	67
BIBLIOGRAPHY.....		69

## LIST OF FIGURES

Figure 2-1: Classification of elastic waves in concrete pipe .....	7
Figure 2-2: Schematic of IE and ACIE method.....	8
Figure 3-1: Representation of low-, medium-, and high-frequency wavelets and their frequency spectrums. ....	17
Figure 3-2: Schematic of numerical model used to simulate ACIE in a fluid filled concrete pipe (without soil cover).....	18
Figure 3-3: Mesh refinement study: (a) Elastic domain and (b) Acoustic.....	20
Figure 3-4: Schematic of the 3D numerical model.....	21
Figure 3-5 Sketch of the FEM model with concrete pipe surrounded by soil layer. ....	22
Figure 3-6: Enlarged 2D image of the IE response of the concrete pipe without the surrounding soil layer. ....	24
Figure 3-7: 2D graphs of the IE response of concrete pipe a) 300 $\mu s$ , b)600 $\mu s$ , c)900 $\mu s$ . ....	25
Figure 3-8: Transient response of 2D concrete pipe a) waveforms, b) frequency spectra. ....	26
Figure 3-9: Transient response of 3D concrete pipe: a) waveforms, b) frequency spectra.. ....	27
Figure 3-10: Comparison of the thickness frequency with different material properties.....	28
Figure 3-11: 2D plots of IE response of concrete pipe a) 300 $\mu s$ , b)600 $\mu s$ , c)900 $\mu s$ . ..	30
Figure 3-12: Transient response of 2D concrete pipe for soil A: a) Time domain waveforms, b) Frequency spectra. ....	31
Figure 3-13: Transient response of 2D concrete pipe for soil B: a) Time domain waveforms, b) Frequency spectra .....	32
Figure 4-1: Concrete pipe samples. ....	35

Figure 4-2: A photograph of experimental setup: a) RCP specimen A b) Close up.....	36
Figure 4-3: Schematic of experimental setup .....	37
Figure 4-4 Frequency spectrum of IE and ACIE measurements .....	38
Figure 4-5 A normalized frequency spectrum with variation of height of microphone. ..	39
Figure 4-6 Variation of thickness frequency along length of pipes a) sample A b) sample B.....	41
Figure 4-7 Thickness frequency obtained using the measured mechanical properties.....	42
Figure 4-8 Design of sound insulation enclosure .....	43
Figure 4-9: Developed spray foam noise suppressor .....	43
Figure 4-10: Comparison of frequency spectrum for enclosure and without enclosure condition. ....	44
Figure 4-11: Schematic of experimental setup of the buried concrete pipe. ....	45
Figure 4-12: Experimental setup for buried concrete pipe. ....	46
Figure 4-13: Frequency response of concrete pipe segment without soil layer.....	47
Figure 4-14: Frequency response of the concrete pipe sample segment with the surrounding layer of soil. ....	48
Figure 5-1: Block diagram of the circuit.....	51
Figure 5-2: The input waveform for excitation.....	52
Figure 5-3: Schematic of experimental setup .....	52
Figure 5-4: Photograph of the (a) experimental setup (b) Close-up showing microphone, accelerometer, and solenoid impactor (c) solenoid impactor (d) Impactor and MEMS microphone.....	53
Figure 5-5: Frequency spectrum obtained using condenser and MEMS mic.....	53
Figure 5-6: Frequency spectrum obtained using MEMS microphone's (a) Raw data (b)Filtered data.....	55
Figure 6-1: Thickness loss due to corrosion .....	58
Figure 6-2: Delamination of concrete deck slab.....	59

Figure 6-3: Illustration of flaws (a) thickness loss (b) delamination (c) Fluid filled void. ....	60
Figure 6-4: Frequency spectrum of thickness loss flaw for: a) acoustic domain b) elastic domain .....	62
Figure 6-5: Frequency spectrum for delamination defect for a) acoustic domain b) elastic domain. ....	63
Figure 6-6: Influence of sizes of voids on thickness frequency response (a) Acoustic domain (b) Elastic domain. ....	64

## LIST OF TABLES

Table 3-1: Elastic properties of concrete .....	19
Table 3-2: Types of soil installation .....	23
Table 3-3: Properties of soil .....	23
Table 3-4: Summary of results from a standalone pipe .....	27
Table 3-5: Effect of different material properties of pipe on thickness frequency .....	29
Table 4-1: Dimensions RCP pipe segments.....	35
Table 6-1: Elastic properties of concrete and soil .....	61

## **ACKNOWLEDGMENTS**

I thank Dr. Arun Jaganathan for allowing me to conduct research under his supervision. I am greatly indebted to all the support and guidance at each step of the research program.

# CHAPTER 1

## INTRODUCTION

### 1.1 Background and motivation

Concrete pipelines constitute a critical part of the buried infrastructure. It comes in several types including Reinforced Concrete Pipes (RCP) and Prestressed Concrete Cylinder Pipes (PCCP). The bulk of these pipes have outlived their design life and must be repaired [1], and non-destructive testing (NDT) plays a crucial role in this repair process. The American Society of Civil Engineers (ASCE) gives a grade of “D” for the overall condition and capacity of the nation's wastewater infrastructure in its 2021 report, indicating a need for significant improvement and maintenance [2]. The U.S. Environmental Protection Agency (EPA) estimates that more than \$743 billion in investments will be needed by the year 2035 to maintain and upgrade this infrastructure [3].

NDT concrete pipes is a mature field. A variety of techniques that are based on several physical principles are available to investigate these pipes. For example, ground penetration radar [4], X-ray [5], thermography inspection [6] with electromagnetic wave [7], are some of the techniques currently available today. Among those, techniques, mechanical (or stress) wave-based methods constitute an important category because we can use them to not only detect subsurface defects but also estimate the material properties of the underlying medium to a certain extent. Among the stress wave methods,

Impact Echo (IE) [8], Spectral Analysis of Surface Waves (SASW) [9], and Multichannel Analysis of Surface Waves (MASW) [10] are that popular methods that are widely employed to test concrete structures in general. These methods allow us to detect subsurface faults like cracks and delamination and the unknown wall thickness, and material characteristics of the structure [11], [12]. However, SASW requires the knowledge of Rayleigh wave velocity of the medium [13]. Since this technique is based on averaging the individual modes to calculate the wave speed, it often introduces errors in the calculations. On the other hand, MASW approach can discriminate individual modes. It has been used recently to calculate the unknown mechanical properties of concrete pipes [14]. However, this method requires data collected using a large number of sensors in order to properly generate the dispersion curve which could be time consuming and labor intensive [15]. Comparatively, IE only requires a single sensor to collect the waveform from a structure and the signal processing required is also relatively easier. Thus, it is the most popular stress wave method used for testing concrete structures.

In IE, the compression wave is induced on the surface of a structure using a ball - hammer. An accelerometer is placed next to the source to receive the signal. Then thickness frequency is computed by transforming the time-domain signal received by accelerometer into frequency domain, from which the resonance (or thickness) is calculated.

The IE method has been used to determine the thickness and subsurface defects in concrete pipes [16], [17]. Thin-walled PCCP pipes have also been investigated [18] and cavities outside sewer pipes have been detected using this method [1]. However, there are certain challenges associated with IE. For example, maintaining an adequate physical



contact between the transducer and the structure is crucial for obtaining reliable results, but this becomes harder in a concrete pipe because of poor surface quality. Improper coupling often results in unreliable results. Thus, a non-contact-based reception of signals becomes important to improve the quality of inspection. There are several ways to capture the signal from a structure without contacting the surface.

One approach to overcome the limitation of IE method is to employ the non-contact-based sensor. To study the attenuation of the concrete-based material a laser and ultrasonic technique has been applied in the past [19]. But employing these techniques due to the poor surface quality which limits the application [20].

Air-coupled IE (ACIE) is an alternative approach that has been investigated for concrete [21], [22]. Where the leaky acoustic waves that accompany the stress waves are captured using a microphone instead of using an accelerometer. While air-coupled reception of acoustic waves in the high ultrasonic frequencies could be difficult to accomplish on a concrete structure, it has been shown the frequencies in the sonic to low ultrasonic range less than 60 kHz can be effectively captured on concrete [23].

ACIE has been investigated for NDT of concrete structures such as bridge decks [24], [25], pavement [26]. However, it has not been explored for concrete pipes yet. Thus, the objective of this project is to investigate ACIE as a tool for the NDT of concrete pipes. While the primary objective of this research is to replace the contact-based receiver used in IE with a non-contact transducer (microphone), the impact source is still manually operated, and it is difficult to control the impact force via manual ball hammer. In past, electrically and pneumatically actuated impactors employed for IE to

overcome this limitation [27] . Therefore, to produce the impact in controlled fashion a semi-automated ACIE system using solenoid impactor is also explored.

## **1.2 Objectives**

The overall goal of this research is to investigate the feasibility of ACIE technique as a tool for the NDT of buried concrete pipes. Research conducted here is limited to RCP pipes only. The investigations are carried out in four stages:

- I. First a feasibility study is conducted numerically by simulating ACIE in an RCP pipe using the finite element-based tool.
- II. The proof- of – concept experimental demonstration is conducted using laboratory experiments. The experimental results are used to validate the numerical results.
- III. Detailed parametric study to find optimal location of microphone with the pipe has been completed.
- IV. Investigation to suppress noise and improve signal to noise ratio has been completed.
- V. A semi-automated test setup is developed to enable ACIE implementation in a compact, cost effective and rapid tool.
- VI. Analyze practical ability to detect common pipe wall defects.

## **1.3 Dissertation outline**

This dissertation has seven chapters. Chapter 1 contains introduction, objectives, and organization of the dissertation.

Chapter 2 describes working principle involved for conventional IE and ACIE

techniques.

Chapter 3 discusses the introduction to numerical simulation using time domain based Finite element modeling.

Chapter 4 discusses experimental work and the results obtained from lab work. Two RCP pipe segments have been tested and proof-of-concept for experimental demonstration conducted using laboratory experiments.

Chapter 5 describes a semi-automated ACIE system developed using MEMS microphone.

Chapter 6 discusses the feasibility of ACIE technique to detect common pipe wall defects using numerical modeling.

Chapter 7 provides the summary with discussion of the conclusions.

## **CHAPTER 2**

### **IMPACT ECHO AND AIR COUPLED IMPACT ECHO: AN OVERVIEW**

Impact echo (IE) is a well-known non-destructive testing (NDT) method that is widely used to evaluate the condition of concrete structures including tunnel [28], beam [29], bridge decks [30]. It is a fast, reliable, and cost-effective method for assessing the condition of concrete without damaging structure. In the past, this method has been extensively used to investigate plate-like structures. Here we focus on pipes. When a concrete pipe is excited with a point impact (steel ball), it results in the production of two different types of guided waves that move along the length of the pipe and along the circumference [10] as shown in Figure 2-1. These waves are referred to as the longitudinal wave and circumferential wave, respectively. Apart from these guided waves, however, there is also a local resonance of P-wave across the pipe wall beneath the impact location. When P-wave reaches the inner and outer surfaces of the concrete pipe, they reflect off of these surfaces and create multiple reflections. Thus, a local resonance is produced. This resonance frequency is called as the thickness frequency [31]. IE testing is able to detect small defects that may not be visible from the surface. Defects such as cracks, delamination's, voids can be detected by the IE and unknown wall thickness can be calculated.

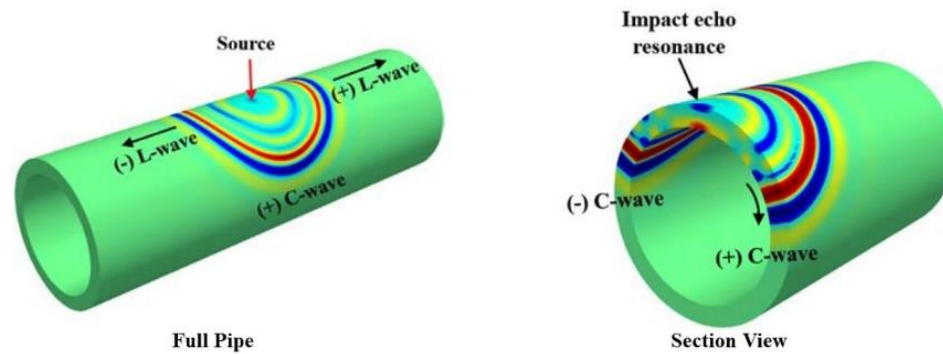


Figure 2-1: Classification of elastic waves in concrete pipe [10]

The P-wave velocity ( $V_p$ ) in an isotropic and linear elastic material is related to mechanical properties is given by [32]:

$$V_p = \sqrt{\frac{E(1-\nu)}{\rho(1+\nu)(1-2\nu)}} \quad \text{Eq. 2.1}$$

where,  $E$  is Young's modulus of elasticity,  $\rho$  is density,  $\nu$  is the Poisson's ratio.

Earlier impact echo studies were primarily conducted in the time domain, which involves measuring the response of the structure to the applied impact in terms of time. However, over time, researchers found that frequency analysis can provide more detailed and accurate information about the structure condition [33]. By analyzing the response of the structure in frequency domain, it is possible to identify the specific frequency at which the P- wave resonates. Additionally, frequency analysis can also help to filter out noise and unwanted signals, which can improve the overall accuracy of the test. A general schematic of IE and ACIE is represented in Figure 2-2.

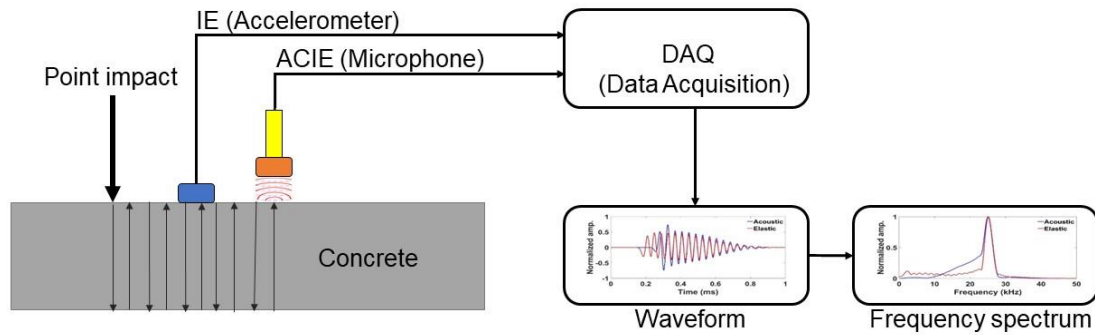


Figure 2-2: Schematic of IE and ACIE method

While in IE test an accelerometer is used to capture the surface displacements and in ACIE testing a microphone is used to capture the acoustic wave induced. Both transducers are placed near the source of the impact. The transducer converts the mechanical motion of the structure into the electrical signal, which is then recorded in the time domain. Then it is converted into a frequency spectrum using Fast Fourier transformation (FFT). The thickness frequency  $f_t$ , the unknown thickness ( $h$ ) of the structure is calculated using following [33]:

$$h = \frac{V_p}{2f_t} \quad \text{Eq. 2.2}$$

Later on, to overcome the discrepancy with the experimental data, an empirical correction factor ( $\beta$ ) was introduced to improve the accuracy as [34]:

$$h = \frac{\beta V_p}{2f_t} \quad \text{Eq. 2.3}$$

There are three unknowns in the above equation i.e.,  $V_p$ ,  $h$ , and  $f_t$  and knowledge of two is required to calculate third. In this study, the  $V_p$ , that was determined through the

application of the multichannel analysis of surface waves (MASW) technique was used [10].

If the pipe has multiple layers, the amplitude of the reflected ( $A_{ref}$ ) and transmitted ( $A_{tran}$ ) wave at an interface between two mediums can be calculated using the difference in their acoustic impedances according to Equation 2.3 and 2.5 [17]:

$$A_{ref} = \frac{Z_2 - Z_1}{Z_2 + Z_1} \quad \text{Eq. 2.4}$$

$$A_{tran} = \frac{2Z_2}{Z_2 + Z_1} \quad \text{Eq. 2.5}$$

where,  $Z_1$  &  $Z_2$  are acoustic impedance of two mediums. For example, if medium 1 is concrete with an acoustic impedance  $9.2 * 10^6 \text{ kg/m}^2\text{s}$  and medium 2 is soil with an acoustic impedance of  $1.6 * 10^6 \text{ kg/m}^2\text{s}$ , then for a P-wave inside i.e., at the concrete/soil interface, approximately 67 % of the wave energy is reflected and the remaining 33 % is transmitted through the interface. However, at concrete/air interface, approximately 100 % of the wave energy is reflected due to huge difference in acoustic impedance.

## 2.1 Instrumentation

Instrumentation used in IE method is composed of three main components: the impactor, the receiving transducer, and data acquisition system. These components are described next.

### 2.1.1 Impactor

Pipe is excited by an impactor. Several types of impactors including steel ball hammer, piezoelectric actuator, or pneumatic actuator are used to excite the pipe. Steel balls are relatively inexpensive and widely used for IE testing. The frequency content generated by a steel ball is related to contact time ( $t_c$ ) of the impact hammer. Typically, the contact time of the impact varies from 20  $\mu$ s to 80  $\mu$ s [35]. Diameter of the ball is another factor that influences the maximum frequency generated and can it be estimated using the following set of equations [18]:

$$f_{max} = \frac{1.25}{t_c} \quad \text{Eq. 2.6}$$

$$t_c = 0.0043d \quad \text{Eq. 2.7}$$

where,  $d$  is the diameter of the ball. It can vary from 3 mm to 19 mm. A small-diameter ball hammer can produce higher frequencies than a large ball. So, the ball has to be chosen carefully to such that the frequency content produced is higher than the thickness frequency expected.

### 2.1.2 Transducer

The time-domain signal generated in the pipe recorded by a broadband displacement-based transducer, like an accelerometer which require physical contact to the surface. For non-contact recording, microphones are utilized. A brief description of these two are given next.

### 2.1.3 Contact transducer

These transducers are attached to the pipe surface to measure the surface displacement induced due to elastic waves. They have a piezoelectric element inside a housing that senses mechanical vibrations and turns them into electrical signals. To



effectively apply this technique, the transducer should be properly coupled to the surface. However, this often becomes a difficult task due to the poor surface quality of the concrete. This issue can be addressed through surface preparation or by using adhesive mounting techniques.

The placement of the transducer is also crucial. If the source and receivers are positioned too far apart, good quality signal may not be captured. The optimal distance between them should be about 0.2 to 0.4 times the thickness of the pipe [34].

#### 2.1.4 Non-contact transducer

Non-contact transducers do not require surface preparation and microphones are commonly used to record leaky acoustic waves accompanying the elastic wave. In general, the magnitude of this wave is much lower due to acoustical impedance mismatch between air and solid. So, the signal has to be amplified electronically. Signal processing techniques used here are similar to a contact transducer. Dynamic and condenser microphones are commonly used for this purpose. Micro-Electro-Mechanical Systems (MEMS) microphones are increasingly gaining attention because to their miniature size and low price and high sensitivity [36].

#### 2.1.5 Data acquisition system (DAQ)

A data acquisition system is the last component used. For laboratory testing, an oscilloscope was used as DAQ along with a signal conditioner and a computer. The signal conditioner amplifies, filters and conditions the signals prior to sending it to oscilloscope.

In this chapter, the basic principles of IE and ACIE techniques were discussed. The next chapter will deal with numerical modeling of these techniques.

## **CHAPTER 3**

### **NUMERICAL MODELLING OF AIR COUPLED IMPACT ECHO**

#### **3.1 Introduction**

This chapter describes numerical modeling of IE and ACIE method. Finite Element Method (FEM) is widely used for modeling elastic and acoustic wave propagation [37], [38]. The elastic waves propagate on the concrete surface. However, concrete is inhomogeneous material and scattering of these waves caused by pores and aggregates, has been shown to have a lower significance in impact echo measurements at frequencies below 60 kHz compared to higher frequencies between 60 kHz and 200 kHz [23]. The maximum frequency generated by a steel ball impact on concrete is typically around 50 kHz [10]. Thus, this study has assumed that concrete as well as soil a linear elastic, isotropic and homogeneous material for the purpose of testing at frequency below 60 kHz.

In the beginning a 2D model of ACIE is developed using COMSOL Multiphysics. Then it is expanded to a 3D model. The outcomes (thickness frequency) calculated from models are compared. A parametric study is then performed by changing the mechanical properties of pipe. The feasibility of ACIE in buried pipes was examined. The effect of two types of soil cover around the pipe was analyzed.

### 3.2 Governing equations

In an elastic-acoustic system, waves in solid structures are governed by the Navier stocks equation. In fluids, waves are described by the scaler wave equation. At the interface between two mediums, continuity conditions are applied. The domain is terminated in buried pipe model using absorbing boundary conditions (ABC) to simulate in finite domain and to prevent unwanted reflections from the boundary. Next, the governing equations and boundary conditions that were implemented are discussed briefly.

#### 3.2.1 Elastic domain:

Under the assumption of small deformation, the material was modeled as a linear elastic domain with isotropic properties. The stress-strain relationship for an isotropic material is described by the following constitutive matrix equation [39]:

$$\sigma_E = C_E \cdot \varepsilon_E \quad \text{Eq. 3.1}$$

where  $\sigma_E$  is Cauchy stress tensor,  $\varepsilon_E$  is strain tensor and  $C_E$  is the constitutive matrix. For a linear elastic material with isotropic properties, the stress and strain tensor are related by the constitutive matrix and its components are given by:

$$C_E = \begin{bmatrix} \lambda + 2\mu & \lambda & \lambda & 0 & 0 & 0 \\ \lambda & \lambda + 2\mu & \lambda & 0 & 0 & 0 \\ \lambda & \lambda & \lambda + 2\mu & 0 & 0 & 0 \\ 0 & 0 & 0 & \mu & 0 & 0 \\ 0 & 0 & 0 & 0 & \mu & 0 \\ 0 & 0 & 0 & 0 & 0 & \mu \end{bmatrix} \quad \text{Eq. 3.2}$$

here  $\lambda$  and  $\mu$  are Lamé's coefficient's and describe the mechanical properties.

They are expressed as the modulus of elasticity,  $E$ , Poisson ratio  $\nu$ , and shear modulus,  $G$  by [40]:

$$\lambda = \frac{\nu E}{(1 + \nu)(1 - 2\nu)} \quad \text{Eq. 3.3}$$

$$\mu = G = \frac{E}{2(1 + \nu)} \quad \text{Eq. 3.4}$$

The governing equation for elastic domain is given by [44]:

$$\tilde{\nabla}^T \sigma_E + b_E = \rho_E \frac{\partial^2 u_E}{\partial t^2} \quad \text{Eq. 3.5}$$

here  $\tilde{\nabla}$  is the differential operator,  $b_E$  is body force (not included in model),  $\rho_E$  is the density,  $u_E$  are the displacements in the elastic domain.

The outer boundary of the pipe is modeled as traction-free when the soil layer is not included. To simulate a buried pipe, PML boundary conditions are applied to the outer boundary of soil[45].

### 3.2.2 Acoustic domain

The acoustic domain is described by the acoustic wave equation, with an assumption that the fluid is compressible and non-viscous. Three differential equations are needed to obtain the acoustic wave equation as mentioned below [41]

The equation of motion:

$$\rho_0 \frac{\partial^2 u_F(t)}{\partial t^2} + \nabla p_F(t) = 0 \quad \text{Eq. 3.6}$$

The equation of continuity:

$$\frac{\partial \rho_F(t)}{\partial t} + \rho_0 \nabla \frac{\partial u_F(t)}{\partial t} = q_F(t) \quad \text{Eq. 3.7}$$

and the constitutive equation,

$$p_F(t) = c_0^2 \rho_F(t) \quad \text{Eq. 3.8}$$

here  $u_F(t)$  is the displacement,  $p_F(t)$  is the dynamic pressure,  $\rho_F(t)$  is the dynamic density,  $q_F(t)$  mass per unit volume,  $\rho_0$  is the density and  $c_0$  is the speed of the sound.  $\nabla$  denotes the gradient of the variable.

The acoustic wave equation, which describes the behavior of sound waves in a fluid, is obtained by combining and linearizing three differential equations is given by [41]:

$$\frac{\partial^2 p_F}{\partial t^2} - c_0^2 \nabla^2 p_F = c_0^2 \frac{\partial p_F}{\partial t} \quad \text{Eq. 3.9}$$

### 3.2.3 Interface between acoustic and elastic domains:

At the boundary between the acoustic and elastic domains, coupling conditions are necessary to ensure continuity of displacements and stresses. The continuity is expressed as [41]:

$$u_{E/n} = u_{F/n} \quad \text{Eq. 3.10}$$

$$\sigma_{E/n} = -p_F \quad \text{Eq. 3.11}$$

where  $u_E$  and  $u_F$  are the displacements in elastic and fluid domain, respectively, and (E denotes elastic domain and F denotes fluid domain),  $\sigma_E$  is the stress,  $p_F$  is the dynamic pressure, and  $n$  denotes the normal component.

The normal displacement components of both domains must be equal at the interface, and (Eq. 3.11) the normal stress in the elastic domain, which must be equal to the negative of the fluid pressure.

## 3.3 Impact

The impact force is the most important aspect of the ACIE test. In previous studies, several force functions were utilized to approximate the force injected into the pipe [42], [43]. A steel ball is used as an impactor to generate elastic waves. As

mentioned in Chapter 2, the highest frequency that can be excited by this impactor given by (Eq. 2.6 and Eq.2.7) depends on the diameter. For example, a 10 mm steel ball will generate the highest frequency of around 29 kHz, which can be influenced by the duration of the point impact. The duration of impact on concrete affects the frequency range generated due to vibration. As it shortens, the generated pulse contains higher frequency (shorter wavelength) components. However, pulses produced by shorter duration impacts have limited penetration ability in concrete. Therefore, it should be selected in such a way that the generated pulse contains wavelengths greater than the thickness of the structure [33].

There are different force functions used to simulate point impact in the literature including half-cycle sine curve [44], the first derivative of the Gaussian pulse [45], and the Ricker wavelet (also known as the second derivative of the Gaussian function) [46]. Of these, the Ricker wavelet is preferred because it does not have DC content. In addition, the frequency generation can be controlled by a single variable that represents peak frequency [47]. It is defined by the following equation [48]:

$$F(t) = (1 - 2\pi^2 f_p^2 t^2) e^{-\pi^2 f_p^2 t^2} \quad \text{Eq. 3.12}$$

where,  $f_p$  is the peak frequency of the spectrum. The impact is applied normal to the surface of the structure. It is crucial to choose the appropriate  $f_p$  so that it represents actual spectral content generated. Three synthetic wavelets are presented in Figure 3-1 to study low ( $f_p = 5 \text{ kHz}$ ), medium ( $f_p = 10 \text{ kHz}$ ) and high ( $f_p = 15 \text{ kHz}$ ) and their corresponding spectrum. The low  $f_p$  covers up to 16 kHz, medium up to 32 kHz and high  $f_p$  cover up to 47 kHz of the frequency range.

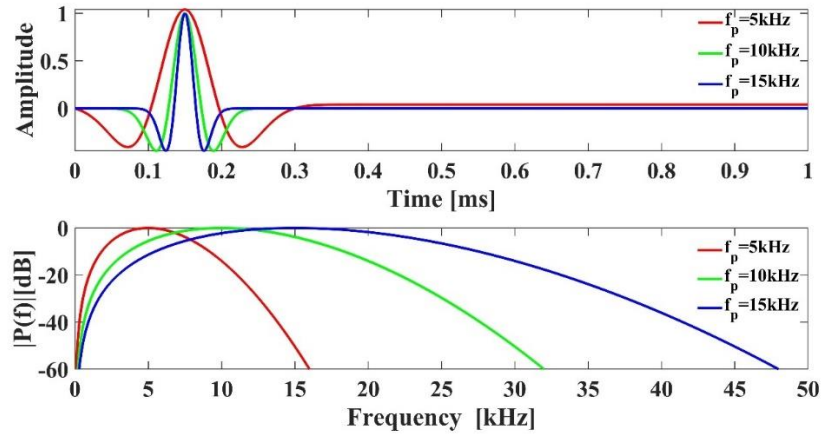


Figure 3-1: Representation of low-, medium-, and high-frequency wavelets and their frequency spectrums.

### 3.4 Computational mesh size and time steps

In numerical modeling, selecting appropriate time step ( $\delta t$ ) and mesh size is crucial to obtain accurate results. Finer mesh will provide accurate solutions; however, it will also require more computational resources [49]. Therefore, it is crucial to strike a balance between the accuracy and computational time requirements. The integration time step is selected according to the following equation [50]:

$$\delta t = \frac{1}{20f_{max}} \quad \text{Eq. 3.13}$$

where  $f_{max}$  denotes the highest frequency of interest. In addition to the integration time step another important factor is the size of the elements, denoted by the notation  $l_e$ . An equation used to determine the appropriate mesh element size is mentioned following [50]:

$$l_e = \frac{\lambda_{min}}{N} \quad \text{Eq. 3.14}$$

here  $\lambda_{min}$  is the shortest wavelength and N denotes the number of elements per wavelength. A wide range of N is found in the literature including 6 [51], 10 [52], and 20 [50]. A mesh refinement study is performed to choose the appropriate mesh element size for the numerical model (described later).

### 3.5 Model 1: 2D model with a standalone pipe

Figure 3-2 illustrates the simulation of pipe model filled with fluid. Concrete is represented as an elastic domain and cavity is represented by the acoustic domain. The dimensions of pipe used is 0.76 m in outer diameter and 0.68 m in inner diameter. This represents a commercially available RCP [53]. These pipes are often used for storm drains and sewer systems.

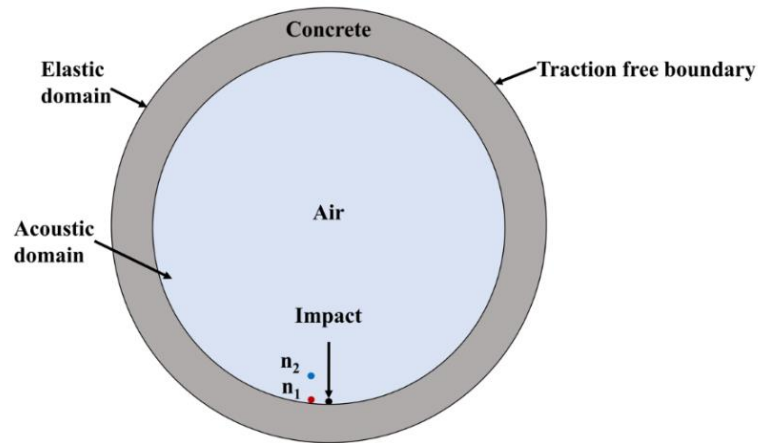


Figure 3-2: Schematic of numerical model used to simulate ACIE in a fluid filled concrete pipe (without soil cover).



The outer boundary is treated as traction-free. Impact point and transducer should be 0.2 to 0.4 times the thickness of the pipe [54]. Impact force was applied to the bottom of the pipe to record the elastic and acoustic domains near the impact point at two nodes,  $n_1$  (elastic) and  $n_2$  (acoustic). The elastic properties of concrete are tabulated in Table 3-1[35].

Table 3-1: Elastic properties of concrete.

Material	Density (kg/m <sup>3</sup> )	Young's modulus (GPa)	Poisson's ratio
Concrete	2300	33.1	0.2

For simulating the transient impact, a high frequency Ricker wavelet has been used to excite the resonant frequency. A mesh refinement study has been performed to compare the thickness frequency obtained for different mesh sizes for accuracy and reliability. For example, Figure 3-3 shows the computed thickness frequency for different mesh sizes for acoustic and elastic domains. The wavelength is related to frequency relation given by:

$$\lambda_{min} = \frac{V}{F_{max}} \quad \text{Eq. 3.15}$$

where  $F_{max}$  is maximum frequency needs to be resolved,  $V$  is velocity i.e., air velocity ( $V_a$ ) and P-wave velocity ( $V_p$ ) is considered 340 m/s and, 4000 m/s, respectively. Using Eq.3.15 the shortest wavelength computed in elastic and acoustic domain is 80 mm and 7 mm. It is necessary to utilize the finest possible mesh to simulate the smallest wavelength in a waveform. This was determined by gradually decreasing the mesh element size from 25 mm to 1 mm for the elastic waves and from 7 mm to 1mm for acoustic waves. The results did not vary significantly when the element size was reduced below 5 mm and 3

mm for elastic and acoustic waves, respectively. The final chosen mesh size is indicated in Figure 3-3a and Figure 3-3b. The simulation was run for 1000-time steps ( $2 \mu\text{s}$ ) for a total duration of 2 ms.

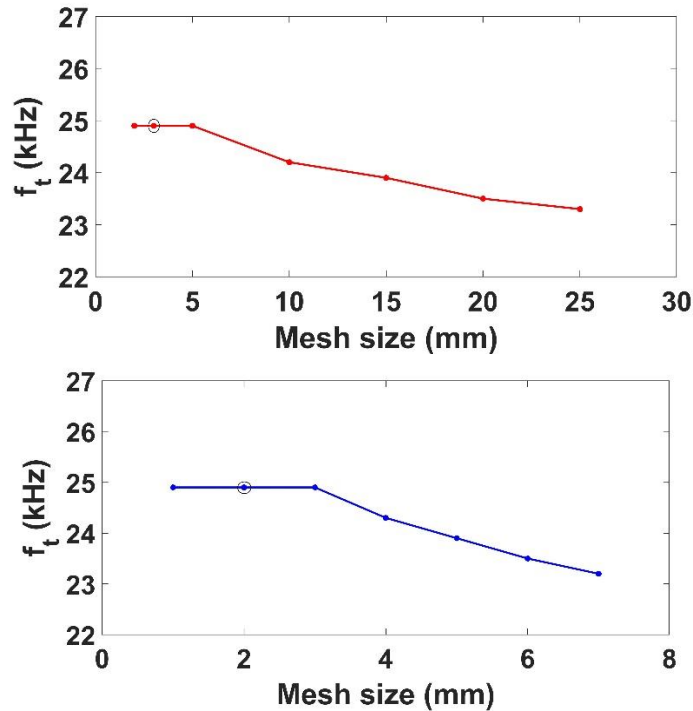


Figure 3-3: Mesh refinement study: (a) Elastic domain and (b) Acoustic.

### 3.6 Model 2: 3D model with a standalone pipe

A 3D model of standalone pipe is developed next. Usually, RCP pipe segments are large, around 2m, to 2.5 m in length as per ASTM- C76 [53]. Since modeling such a large pipe requires a large amount of computer resources. So, the size of the model is reduced by PML boundary. Only a short length of the pipe is modelled. A 0.5 m long segment with a thickness of 0.076 m is considered, as shown in Figures 3-4.

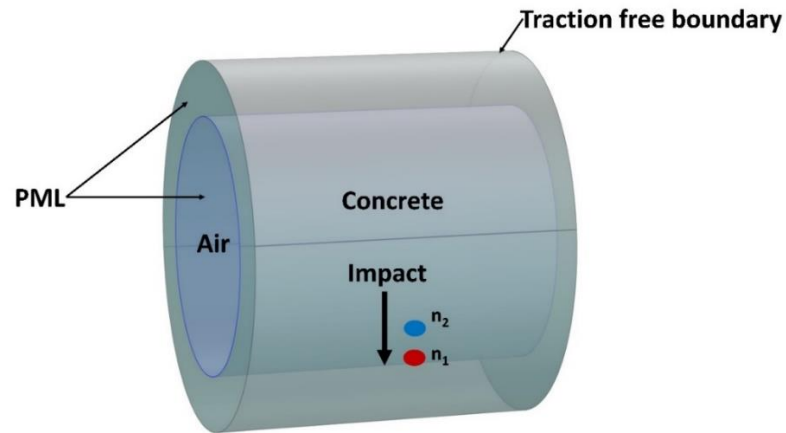


Figure 3-4: Schematic of the 3D numerical model

The impact source is created on the inner surface in the middle at the selected node using Ricker wavelet. Elastic waves are recorded at a distance of 2 cm from the source, and the acoustic signal is collected 2 cm above the surface. The simulation runs for 1000 constant time steps ( $2 \mu\text{s}$ ) for a total duration of 2 ms.

### 3.7 Model 3: 2D model with a buried pipe

Model 1 of the standalone pipe is expanded to include a layer of soil, as shown in Figure 3-5. The outer boundary of the soil is terminated with a PML boundary to simulate an infinite domain.

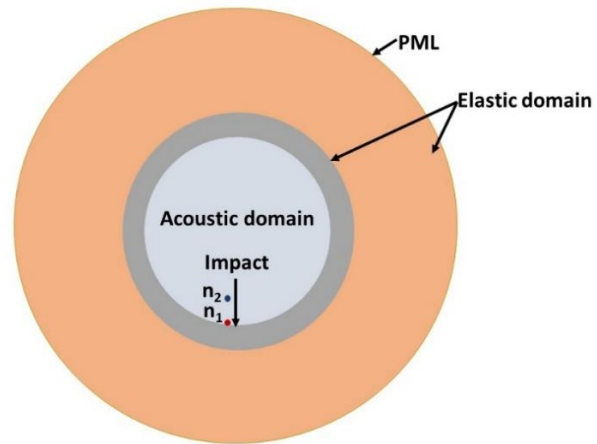


Figure 3-5 Sketch of the FEM model with concrete pipe surrounded by soil layer.

### 3.7.1 Soil properties

The soil surrounding a buried pipe can have varying properties due to factors such as soil type, moisture content, compaction, and construction method used. The type of material and soil compaction level varies depending on the installation type (Type I, Type II, Type III, and Type IV) [55]. The various types of concrete pipe installation are mentioned in Table 3-2:

Table 3-2: Types of soil installation.

Type I	This type requires a well compacted and select granular soil for the bedding zone. This type is cost-effective therefore mostly used for concrete pipe (> 1.5 meters in diameter) buried deep.
Type II:	In this type, native soil is used mainly in the haunch and bedding zones with proper soil compaction. A 3-inch bedside layer is minimally required to save the pipe from placed directly on the hard subgrade.
Type III:	In this type of installation generally, granular, and native soil is used in haunch as well as bedding. Sometimes, adequately silty clay is also used in the haunch zone.
Type IV:	This type is used for the most cost-effective design approach with minimum compaction and backfill requirement except the silty clay soil used in the haunch and outer bedding zone. The clearance between pipe walls and the side of the trench should be greater than outer diameter/6 i.e., > O. D. /6.

Taking the above factors into account, two types of soil, A and B, are chosen for numerical simulation. Their mechanical characteristics are described in Table 3-3[56].

Table 3-3: Properties of soil.

<b>Material</b>	<b>Density (kg/m<sup>3</sup>)</b>	<b>Young's modulus (MPa)</b>	<b>Poisson's Ratio</b>
Soil A	2000	300	0.2
Soil B	2000	138	0.2

The simulation is run for 1000 constant time steps of 2 ms duration with a maximum mesh length of 3 mm in the elastic domain and 2 mm in the acoustic domain.

### 3.8 Results and discussion

#### 3.8.1 Model 1 & Model 2

A snapshot from the numerical model at a specific time step is shown in Figure 3-6. As seen, an elastic wave formed inside the pipe wall leaks into the fluid inducing an acoustic wave.

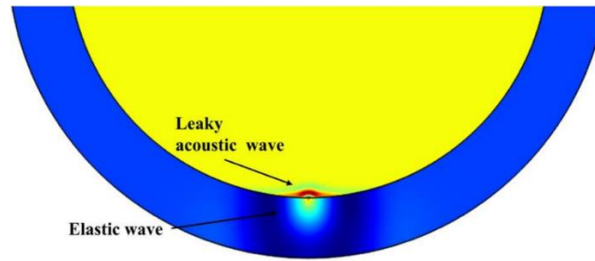


Figure 3-6: Enlarged 2D image of the IE response of the concrete pipe without the surrounding soil layer.

As the stress wave propagates along the wall, it couples with the acoustic wave along the interface. The elastic wave undergoes a resonance near the impact source, and at each cycle a corresponding acoustic response is generated into the fluid. Thus, it is possible to extract the resonance frequency by recording this leaky wave. To further understand its propagation, the output at three different times, i.e., 300  $\mu\text{s}$ , 600  $\mu\text{s}$ , 900  $\mu\text{s}$ , is presented in Figure 3-6. As observed, the acoustic wave emanating from impact point at the bottom of the pipe travels all the way to the top and reflects back. Since pipe acts like a cavity, the acoustic waves could undergo back and forth reflections. It has been noticed that the reflections from the top of the pipe wall do not appear to have any effect on the signal that is received in acoustic as well elastic domain. This is going to take place because the velocity of the leaky acoustic wave in fluid (air) is 340 m/s, and the velocity of the P-wave in concrete pipe is 4000 m/s as mentioned in table 3-1. P-wave velocity is 11 times faster than the velocity of acoustic waves. Thus, the reflections from

the opposite wall take a long time to reach the point where acoustic signal is sampled and this prevents clutter in the data. However, the reflection of acoustic waves may interfere with the signal in both the domains, if the pipe has a smaller diameter.

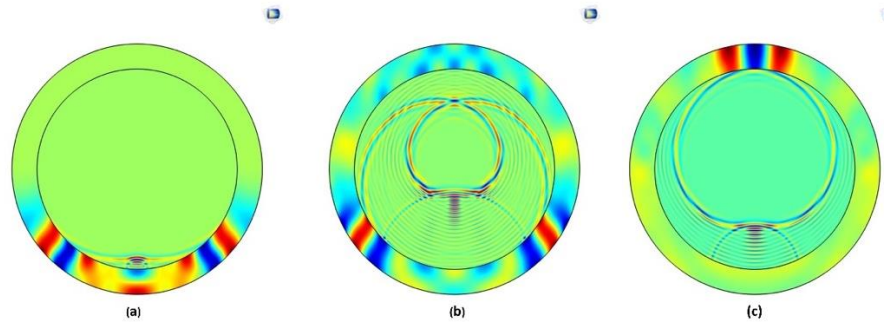


Figure 3-7: 2D graphs of the IE response of concrete pipe a)  $300 \mu s$ , b)  $600 \mu s$ , c)  $900 \mu s$ .

The time-domain waveform is recorded and normalized to obtain frequency spectrums using the Fast Fourier Transform (FFT), as shown in Figure 3-8. The received signals were down sampled using a Hanning window considering 1 ms signal length.

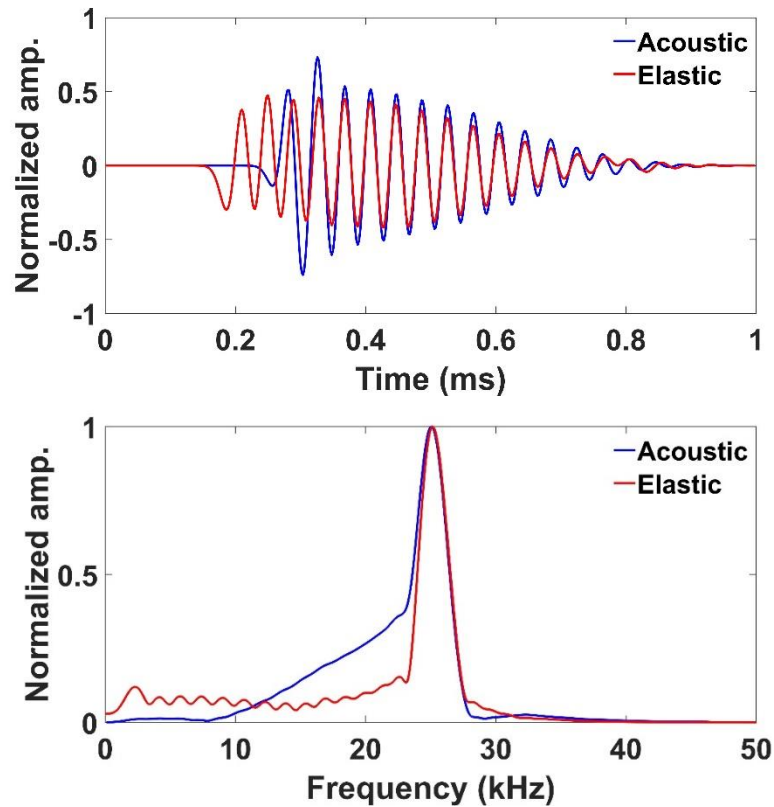


Figure 3-8: Transient response of 2D concrete pipe a) waveforms, b) frequency spectra.

As shown in Figure 3-8b, the elastic and the acoustic domain spectrum had a distinct peak representing the thickness frequency at 24.9 kHz. Using this thickness frequency and the known thickness (used in the numerical model) of the pipe, we have calculated the velocity of the P-wave (3969 m/s). The result was close to the theoretical value of thickness frequency (25.1 kHz) and the velocity (4000 m/s) listed in Table 3-1 with 1% difference. However, model 2 resulted in thickness frequency of 25.2 kHz which was nearest to the theoretical value as shown in Figure 3-9. The results are summarized in Table 3-4.



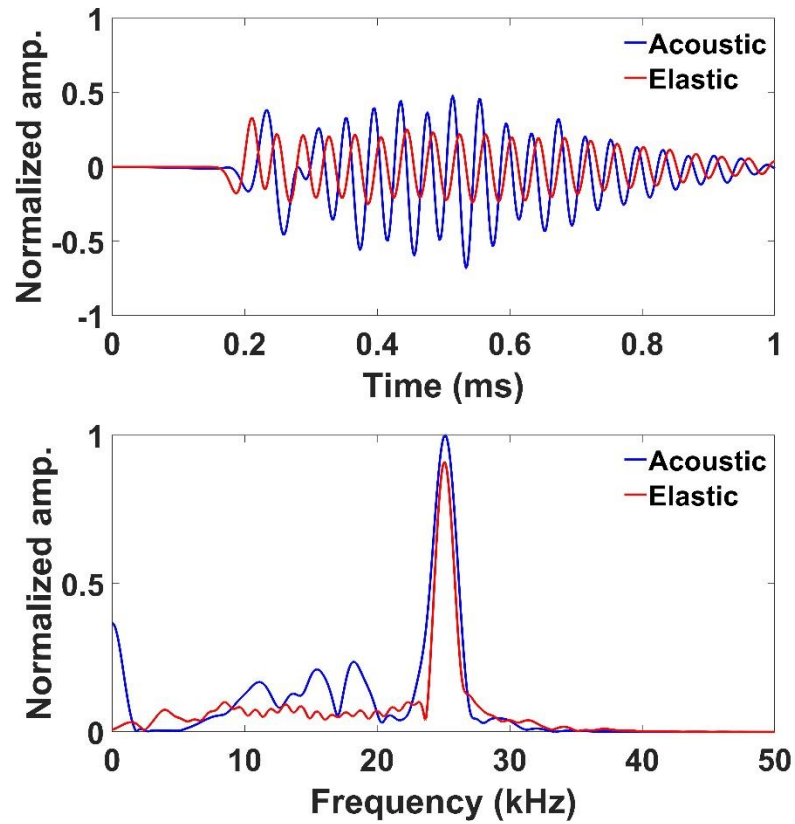


Figure 3-9: Transient response of 3D concrete pipe: a) waveforms, b) frequency spectra.

Table 3-4: Summary of results from a standalone pipe.

Parameters	Model 1	Model 2	Theoretical value
$f_t$ (kHz)	24.9	25.2	25.1
h (m)	0.077	0.076	0.076

In conclusion, results obtained using models 1 & 2 are in agreement. Next a parametric study is conducted for different material properties.

### 3.8.2 Parametric study

Model 1 is used for this study. It involved changing two material properties: Young's modulus from 28 GPa to 38 GPa, and Poisson's ratio from 0.18 to 0.22. The density of the material was kept constant at  $2300 \text{ kg/m}^3$ . Figure 3-10 shows the normalized frequency spectrum with a clear thickness frequency peak. The results showed that the thickness frequency in the elastic and acoustic domains for these two properties were 22.7 kHz to 27.03 kHz, with a difference of concrete modulus.

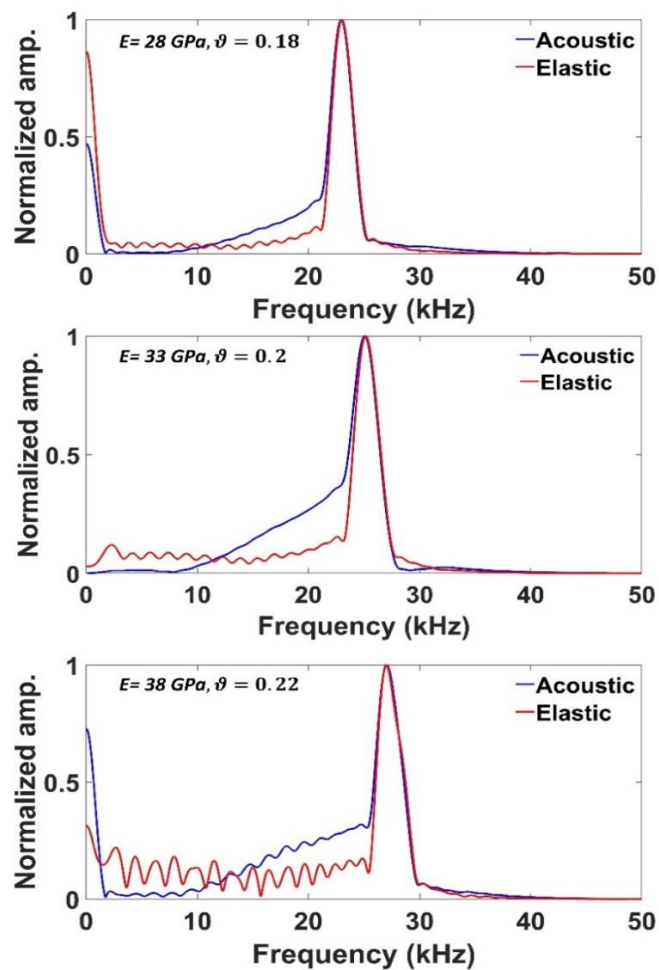


Figure 3-10: Comparison of the thickness frequency with different material properties

The calculation of P-wave velocity using Eq. 2.3 and the thickness frequency results in between 3603.6 m/s and 4343.1 m/s. Further, Pipe thickness was calculated using these velocities and the thickness frequencies as mentioned Table 3-5. The calculated pipe thickness was 0.077 m, which is found to be very close to the known thickness of 0.076 m used in the numerical model.

Table 3-5: Effect of different material properties of pipe on thickness frequency.

S. No.	Young's modulus (GPa)	Poisson' ratio	Density (kg/m <sup>3</sup> )	Thickness frequency (kHz)	P- wave velocity (m/s)
1	28	0.18	2300	22.7	3603.6
2	33	0.2	2300	24.7	3952.8
3	38	0.22	2300	27.03	4343.1

The results showed that the IE and ACIE method can provide accurate results even with variations in the concrete's mechanical properties, demonstrating the method's robustness and reliability of ACIE.

### 3.8.3 Model 3

The study of buried concrete pipe using model 3 is also discussed, with output response at 300  $\mu$ s, 600  $\mu$ s, 900  $\mu$ s, is presented in Figure 3-11. As observed, some amount of energy of waves transferred to the soil at concrete/soil interface.

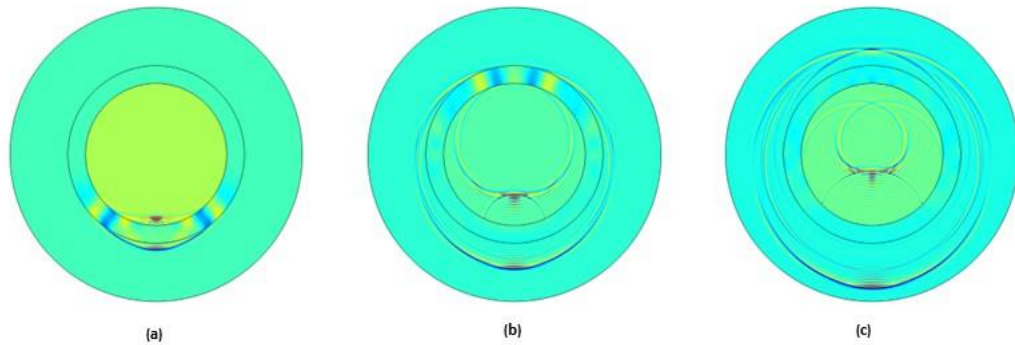


Figure 3-11: 2D plots of IE response of concrete pipe a)  $300 \mu s$ , b)  $600 \mu s$ , c)  $900 \mu s$ .

The signals have been recorded for both Soil A and Soil B in both domains. The frequency spectrums are displayed in Figure 3-12 and 3-13. As observed, energy is transferred to the surrounding soil, leading to a lower amplitude of the IE and ACIE response compared to that of a standalone pipe.

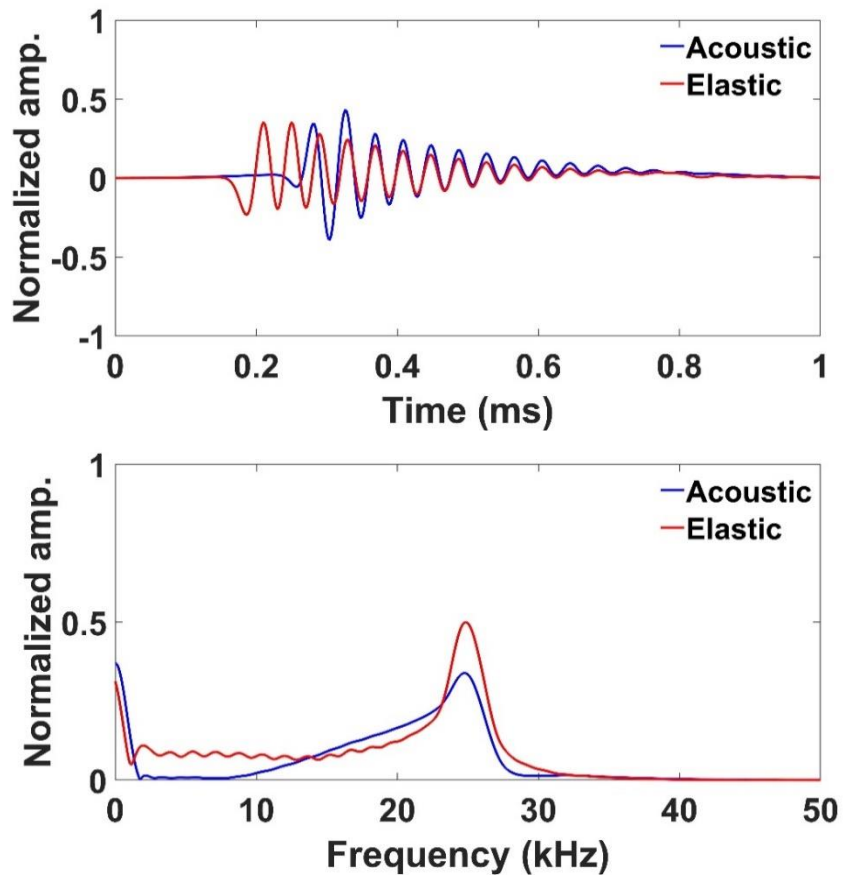


Figure 3-12: Transient response of 2D concrete pipe for soil A: a) Time domain waveforms, b) Frequency spectra.

The results of the study indicate that a significant portion of the incident wave is transmitted into the soil. The transmission coefficient for Soil A and Soil B is calculated as 17 % and 12 %. The transmission coefficient in soil A is higher due to its higher acoustic stiffness. Additionally, the analysis revealed that the normalized amplitude of the wave reflected from the concrete/soil interface in soil A is approximately 50 % in the elastic domain and 34 % in the acoustic domain of the incident amplitude. On the other hand, soil B is less acoustically stiffer. Thus, exhibits improved results in terms of recording the waves in both domains. The wave reflected from soil B has normalized

amplitudes of 80 % in the elastic domain and 40 % in the acoustic domain of the incident amplitude.

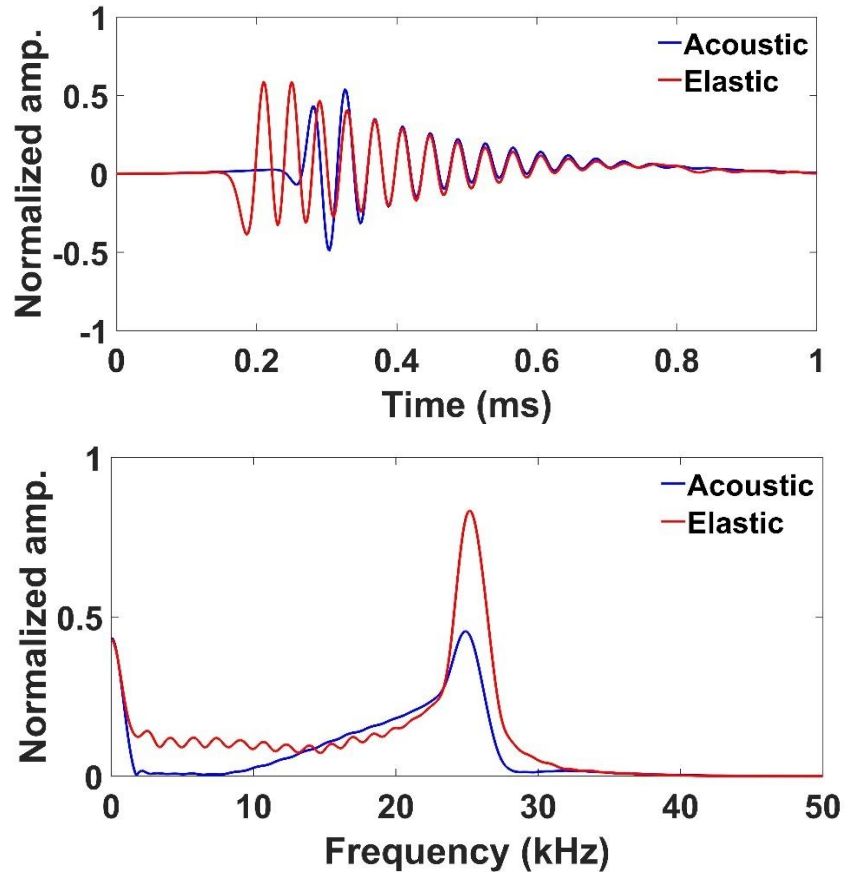


Figure 3-13: Transient response of 2D concrete pipe for soil B: a) Time domain waveforms, b) Frequency spectra

The goal of the study was to determine if leaky acoustic waves could still penetrate the fluid. It was found that the waves were able to reach the fluid domain, despite some energy transfer to the soil at the concrete-soil interface. No reflections were observed from the outside surface of the soil due to the PML boundary condition.

### 3.9 Conclusions

- ACIE was simulated using both a standalone and buried concrete pipe.

- Thickness frequency obtained acoustically match with the results of elastic wave data.
- The presence of soil reduced the amplitude of acoustic signal because of leakage of energy into the soil by about 17 % and 12 % for two soil types tested. However, the amplitude was enough to be detected comfortably.

Overall, this testing method is advantageous because it eliminates the need for mounting a transducer on the surface and can accurately measure leaky acoustic waves in a closed cavity like a concrete pipe without interference from reflections. As a result of these findings, an experimental study was conducted and described in the next chapter.

## CHAPTER 4

### AIR-COUPLED IMPACT ECHO TESTING OF BURIED REINFORCED CONCRETE PIPES: AN EXPERIMENTAL STUDY

#### 4.1 Introduction

This chapter describes the experimental study. Two RCP samples are tested using ACIE technique and the results are compared with conventional IE. Next, a parametric study of the impact of microphone placement over the pipe surface is conducted and optimal height for receiving clean signal is determined. A noise suppressor for microphone is developed to cut down on noise and improve the signal to noise ratio (SNR).

#### 4.2 ACIE testing of standalone pipe segment

In practice pipe can be tested either by entering into it or test it after exploring the surface by removing the soil. The experimental set-up employed in this study is related to the second case.

##### 4.2.1 Instrumentation

Two pipe samples were taken from the construction site and set up in the laboratory as shown in Figure 4-1. Pipe samples meet the ASTM-C76 standards and have a Type B wall [62]. Such pipes are typically used in sewer, industrial waste, and stormwater applications.





Figure 4-1: Concrete pipe samples.

The dimensions of pipe segments are mentioned in Table 4-1.

Table 4-1: Dimensions RCP pipe segments.

<b>Pipe samples</b>	<b>O.D (m)</b>	<b>Thickness (m)</b>	<b>Length(m)</b>
Sample A	0.76	0.07	2.43
Sample B	0.73 to 0.78	0.07 to 0.08	0.58

A manually operated steel ball hammer with a diameter of 8 mm is used as the impactor (Figure 4-2). This ball could generate frequency  $\sim 36.7$  kHz according to Eq. 2.6 and Eq. 2.7. A broadband accelerometer with resonant frequency above 35 kHz is used to receive the elastic waves. It is mounted on the pipe surface using wax to maintain better coupling. A broadband microphone with a frequency range up to 40 kHz is utilized to record the acoustic signal.

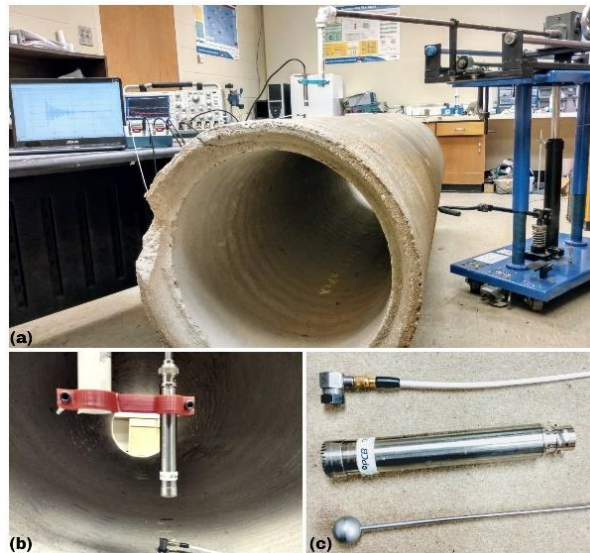


Figure 4-2: A photograph of experimental setup: a) RCP specimen A b) Close up showing location of both transducers c) microphone, accelerometer, and ball impact hammer.

The microphone height was adjusted using the hydraulic table as shown in Figure 4-2. A PCB-480C02 signal conditioner is used to power the transducers and condition the received signals. Figure 4-2 b depicts the positioning of these transducers on the concrete pipe. Figure 4-3 shows a schematic representation of the laboratory equipment used to conduct experiments. Additionally, the signal conditioner connected to an 8-bit oscilloscope (Tektronix MSO 2024) for data acquisition. The data captured by the oscilloscope is transferred to a computer and processed.

The signal is captured within a 10 ms window at a default sampling rate set by the oscilloscope (in MHz) and later it is down sampled using MATLAB. Waveforms are pre-processed by applying a Hanning window, and the spectrum is computed using FFT function.

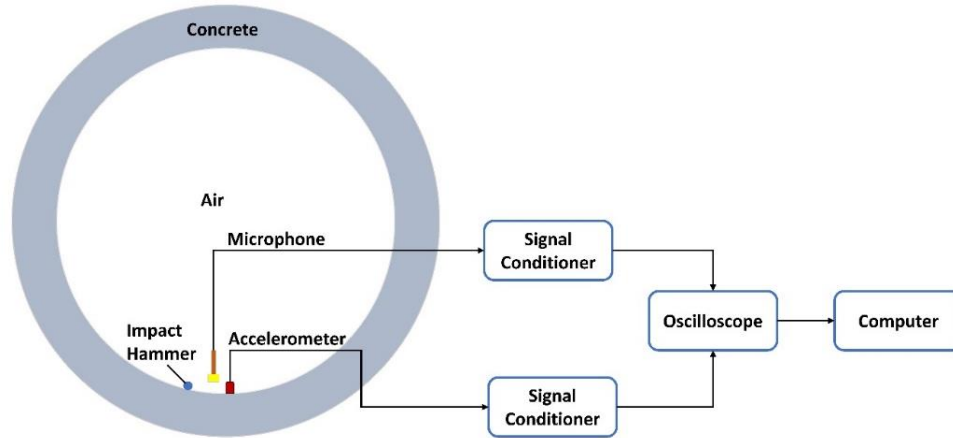


Figure 4-3: Schematic of experimental setup.

#### 4.2.2 Comparison of ACIE and IE results

In traditional IE methodology, the unknown wall thickness can only be determined with prior knowledge of the  $V_p$ . Different methodologies such as SASW and MASW can be used to find the  $V_p$  [57], [58]. For this research, the pipe was characterized using MASW method and  $V_p$  (4433 m/s) [10] obtained by it is used in the IE calculations.

Figure 4-4 illustrates the spectrum contents of the waveforms recorded by the accelerometer and microphone. The thickness frequencies are obtained as 28.18 kHz (accelerometer) and 29.08 kHz (microphone). Data from the accelerometer exhibited lower noise in frequency band up to 20 kHz than that of the microphone as shown in Figure 4-4. This could be due to the effect of direct acoustic wave and environmental noise on the signals received.

Using measured thickness frequency (i.e., 28.18 kHz and 29.08 kHz) and the reported P-wave velocity, pipe thickness is determined to be 0.075 m using accelerometer data and 0.073 m using microphone data. The results differ from the actual value (0.076

m) by 1.32 % and 4.02 % for the accelerometer and microphone, respectively. Which are acceptable. The SNR was then calculated to determine the quality of the received signal.

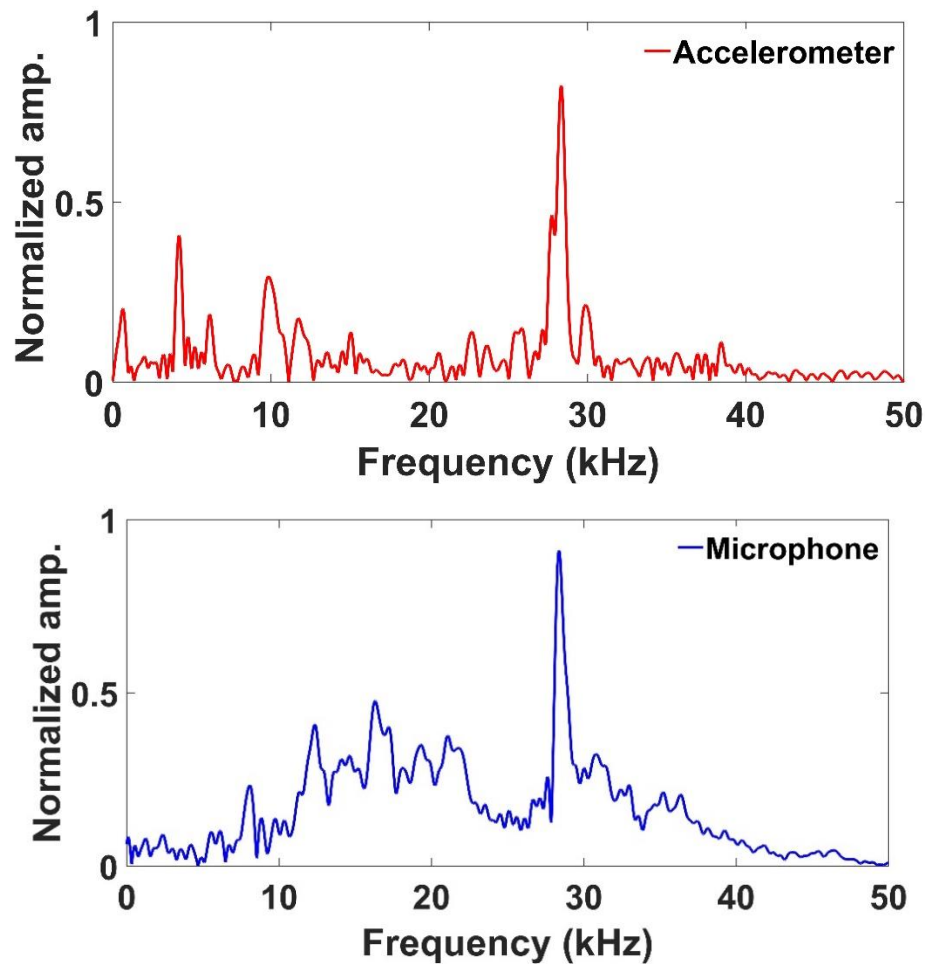


Figure 4-4 Frequency spectrum of IE and ACIE measurements

The ratio of the thickness frequency's amplitude to the noise was computed for both approaches in order to measure the SNR. The relative quality of the signals received was then assessed using this ratio [59].

$$SNR = 20 \log_{10} \frac{Amplitude_{signal}}{Amplitude_{noise}} \quad \text{Eq. 4.1}$$

As shown in the plot in Figures 4-4, the signals from the microphone and accelerometer are estimated to have SNR of 6.23 dB and 5.66 dB, respectively. This

shows that the output of the microphone and the accelerometer provide signal of similar quality.

#### 4.2.3 Parametric study- microphone placement.

In the previous comparison study, it was determined that ACIE test can be used to determine the unknown wall thickness. However, while performing ACIE in the real world, many noises, such as direct acoustic noise and ambient noise, may interfere with the signal [60]. The distances between the microphone and concrete's surface may impact the signal quality. The signal may be distorted if it is positioned too close to the surface. Therefore, optimum placement needs to be established. The microphone is placed at different heights between 0.02 m to 0.07 m from the pipe surface, and results are compared in Figure 4-5.

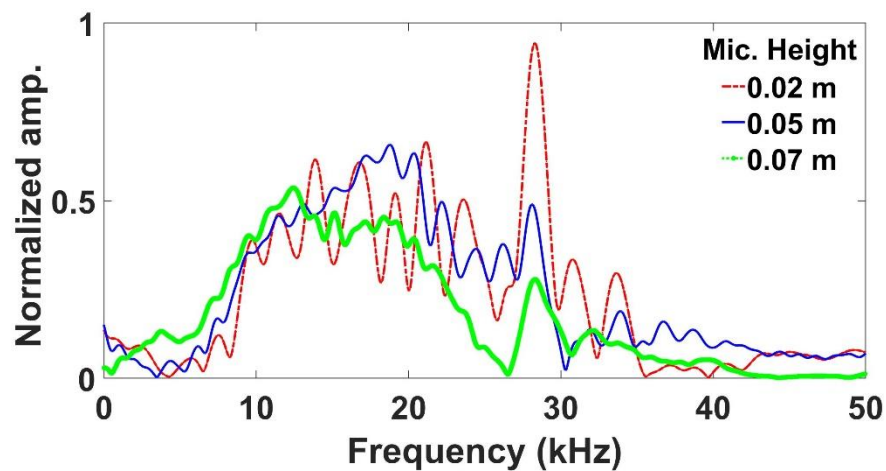


Figure 4-5: A normalized frequency spectrum with variation of height of microphone.

As observed, the amplitude of thickness frequency peak decreases with increasing height, as much as about 60 %. Also, the frequency spectrum reveals a significant amount of noise below 20 kHz. It is possible that the observed effect is caused by the presence of ambient noise and direct acoustic waves. However, the thickness frequency peak is

clearly apparent at the microphone height of 0.02 m. Placing the microphone below this height introduces a higher level of noise. Therefore, a separation between 0.02 m and 0.05 m is the optimal distance.

#### 4.2.4 Characterization of entire pipe

Next the entire pipe was tested by measuring thickness frequency along its length. The test is conducted on the surface at eight successive locations with a spacing of 0.25 m. The distance of the microphone and the impact site is 0.03m.

Figure 4-6a and Figure 4-6b depict the  $f_t$  from two samples tested. It varies within the frequency ranges of 26.01 kHz to 29.13 kHz, 25.10 kHz to 28.45 kHz for samples A and B. Then, the unknown pipe thickness is calculated (with known value of  $V_p$  and  $\beta$  i.e., 0.96).

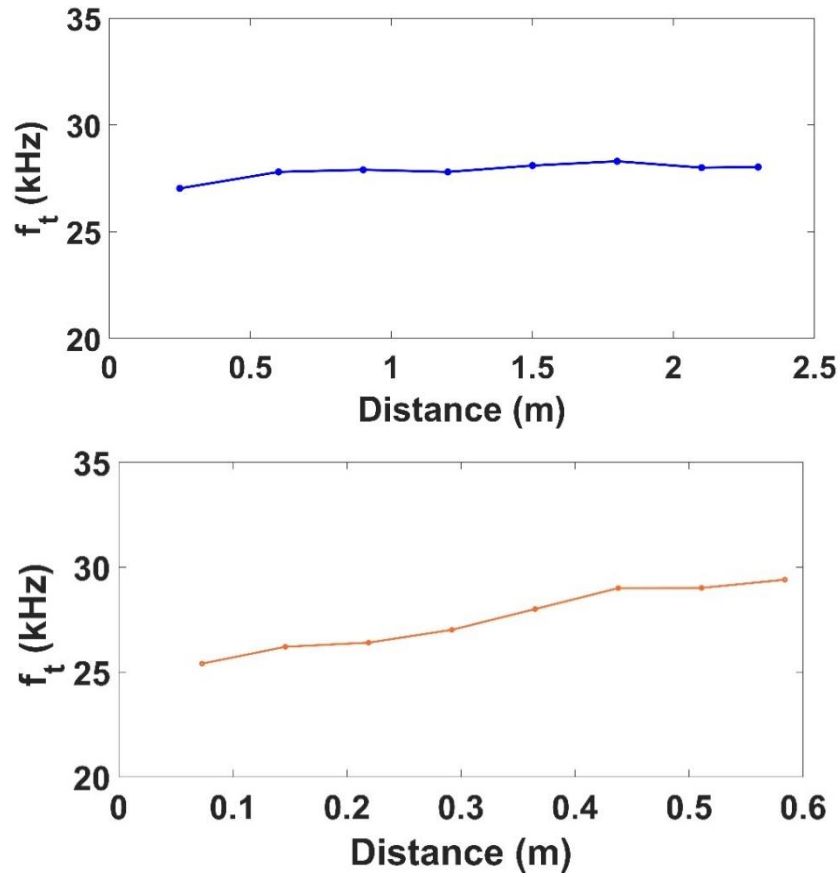


Figure 4-6 Variation of thickness frequency along length of pipes a) sample A b) sample B.

It was found that the calculated thickness varied by 5 % to 6 % from the actual thickness of the pipe (i.e., 0.076 m). On the other hand, we also calculated the P- wave velocity using the known thickness value and measured thickness frequency. It was established that computed  $V_p$  ranged from 4032.1 m/s to 4635.5 m/s, that differed from velocity measured by MASW by 4% to 9%, which is acceptable.

In addition, the measured mechanical properties of pipe are used back in numerical model and thickness frequency was computed (The simulation runs for 2 ms time with 2  $\mu$ s step size for a 1000-time steps). The pre-processing of the signal is done and the signal of 1 ms length was used for frequency analysis as shown in Figure 4-7.

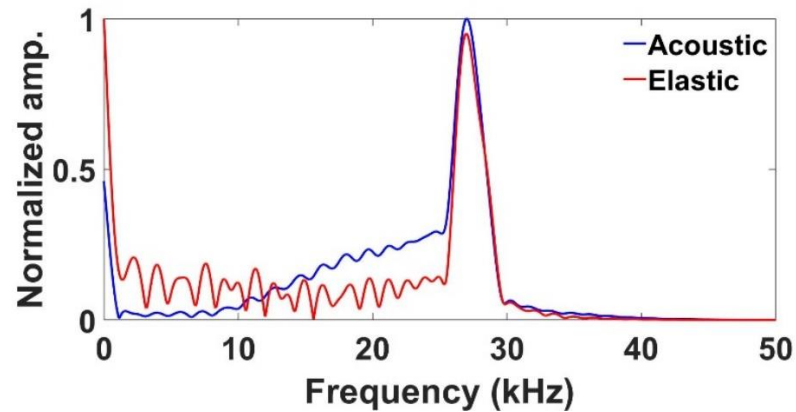


Figure 4-7 Thickness frequency obtained using the measured mechanical properties.

The thickness frequency is clearly evident in the frequency spectrum around 27.3 kHz, which is close to the thickness frequencies observed over the length of both pipe samples.

#### 4.2.5 Design of noise suppressor

To get reliable and consistent results with ACIE, direct acoustic waves and environmental noise must be reduced. Previous research utilized a noise suppressor made from rubber [20] and PVC pipe [36] to reduce the noise. Here, we developed it using high density insulated spray to guard the microphone. It was developed using a closed mold, and it took around 48 hours to get fully cured. The dimensions and arrangement are shown in Figure 4-8.



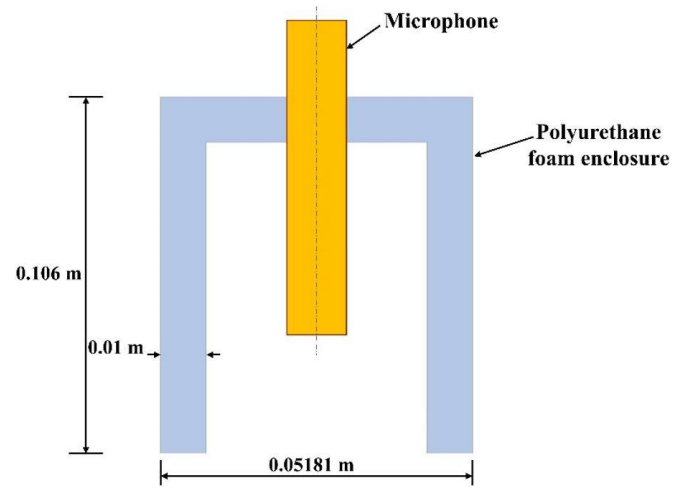


Figure 4-8 Design of sound insulation enclosure.

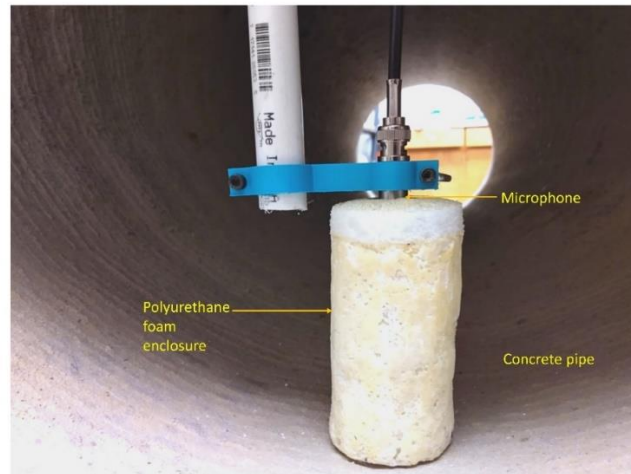


Figure 4-9: Developed spray foam noise suppressor.

The microphone is placed through a hole from the top as shown in Figure 4-9. Its height was chosen between 0.02 m and 0.05 m to effectively capture leaky acoustic waves,

As shown in Figures 4-10, a single dominant peak was noticed to be immediately identifiable in microphone recordings with suppressor and without suppressor condition.

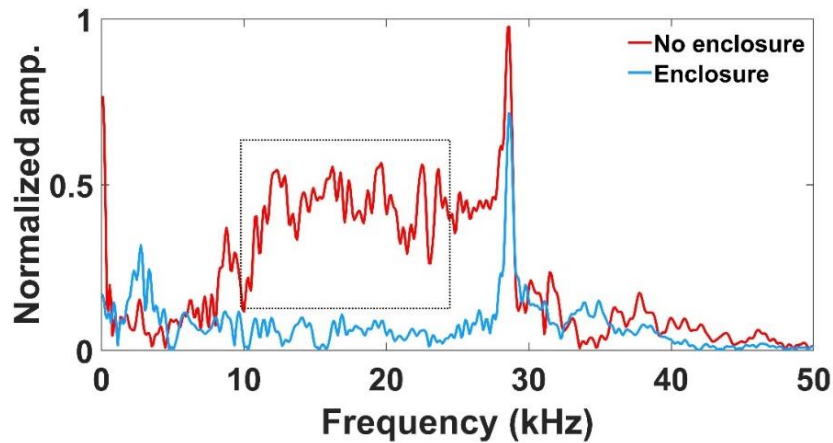


Figure 4-10: Comparison of frequency spectrum for enclosure and without enclosure condition.

In both cases, the frequency spectrum shows that the thickness frequency peak is at 28.08 kHz. Besides the thickness frequency peak the spectrum exhibits multiple unwanted peaks without suppressor. These peaks are present mainly in the 10 kHz -20 kHz frequency band as marked in Figure 4-10. The thickness frequency peak visible distinctly despite slight drop in overall amplitude. Overall, noise is significantly reduced, and SNR is increased to about 13.33. Next, an investigation of buried pipe is presented.

#### 4.2.6 Buried concrete pipe

The schematic of the experimental set-up is shown in Figure 4-11. For convenience sample B (a half-section pipe) is utilized for buried test conditions. The dimensions of pipe sample are listed in Table 4-1.

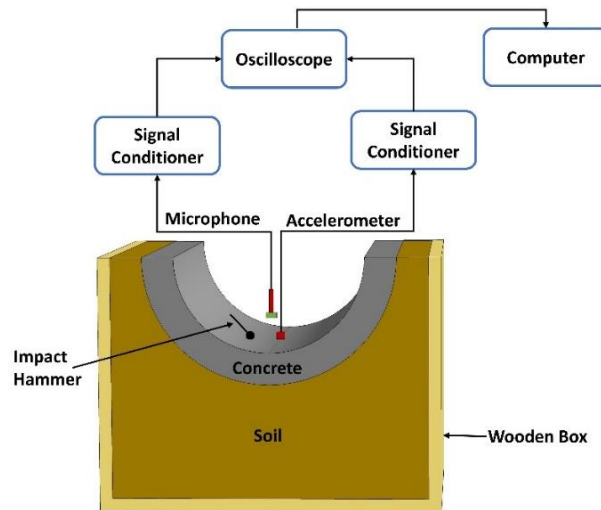


Figure 4-11: Schematic of experimental setup of the buried concrete pipe.

The setup is made in accordance with the type -2 installation using the native soil collected from the construction site. Soil compaction has a significant impact on installation of pipe. Inadequate soil compaction may lead to air voids in the soil which could interfere with the wave transmission and reflection, affecting the signal received. To ensure that the soil is void free, 100 % standard proctor density was employed. The pipe sample is surrounded by a soil layer of 0.35 m thickness in bedding that is similar to that employed for the numerical model. To avoid reflections from the surface of the soil layer, the thickness of soil layer made much larger than the thickness of the pipe.



Figure 4-12: Experimental setup for buried concrete pipe.

The accelerometer coupled to the pipe using wax, and microphone is positioned above it. The impact was produced using an 8 mm diameter ball hammer, and the signals were recorded with a microphone and accelerometer for the ACIE and IE methods, respectively.

#### 4.2.7 Result and discussion

Prior to burying the pipe, data was collected in standalone mode for reference. It was found that the thickness frequency of it varies from 25.10 kHz to 28.45 kHz along the length. A sample spectrum is shown in Figure 4-13. As observed, the frequency spectrum obtained using both the transducers exhibit the thickness frequency at 28.3 kHz. As observed, the microphone data is noisy. It is probably due to end reflections since the sample is short.

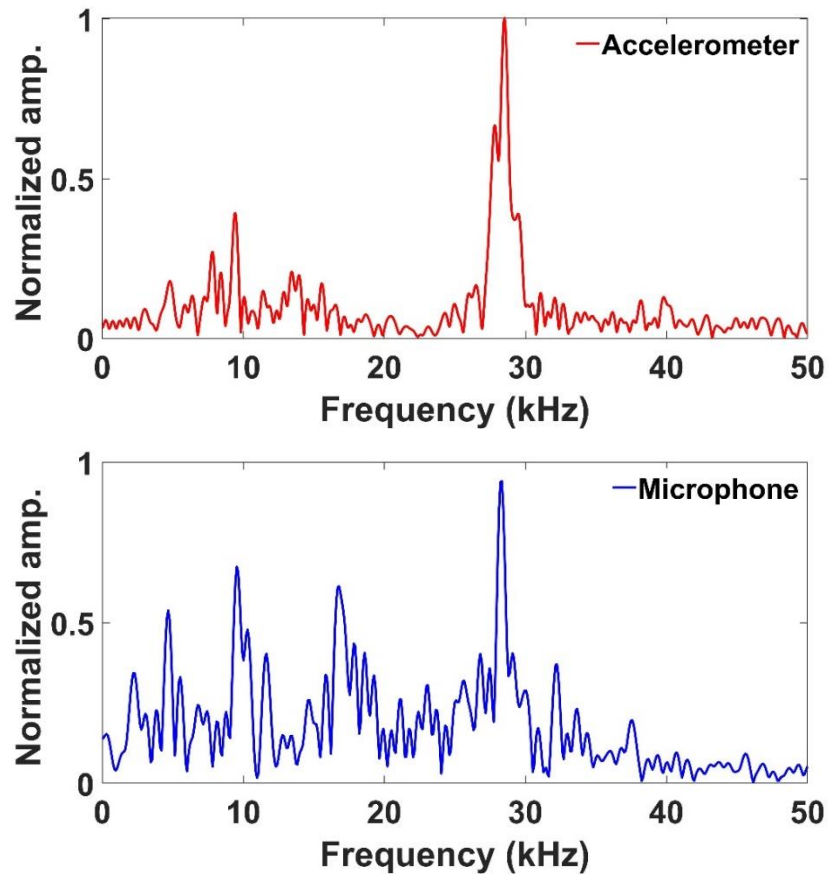


Figure 4-13: Frequency response of concrete pipe segment without soil layer.

Next, the tests were performed with pipe samples surrounded by soil. Figure 4-14 displays the frequency spectrum created using data received from accelerometer and microphone recordings.

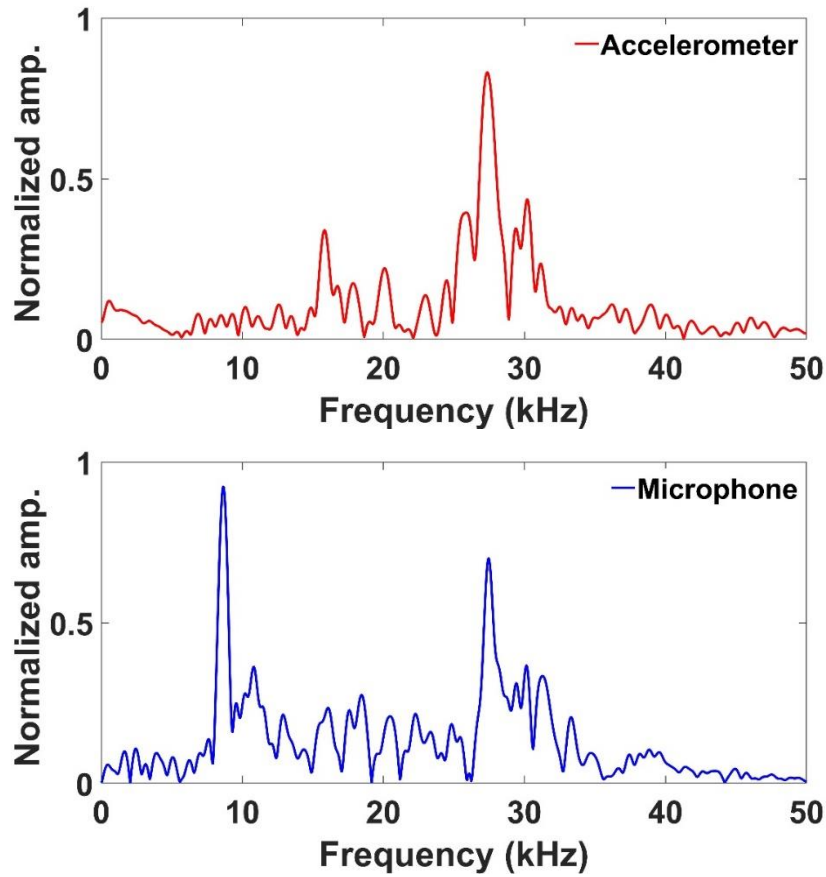


Figure 4-14: Frequency response of the concrete pipe sample segment with the surrounding layer of soil.

The thickness frequency was determined 28.4 kHz for accelerometer and 28.07 kHz for microphone. When compared to the results obtained without a soil layer, the amplitude of the thickness frequency peak reduced by 17 % and 25 %. The majority of the low frequency peaks also seems to have dissipated due to energy loss into the soil.

The test measurement proved that ACIE has the desired performance in terms of sensitivity to capture leaky acoustic waves from buried pipe.

### 4.3 Conclusions

The following conclusions are drawn from the studies:

- It was shown thickness frequency can be measured in a non-contact fashion by measuring the leaky acoustic waves with the microphone. The findings were validated comparing them conventional IE method.
- The parametric study yielded optimal location for the microphone placement. It was found that a separation distance of 0.02 m to 0.05 m is optimal.
- A noise suppressor was developed to enhance the signal received by microphone. It effectively decreased noise and enhanced the SNR by 13.33 dB.
- The ACIE method was also tested using buried samples. The technique can detect leaky acoustic waves even when pipe is surrounded by soil. The amplitude of acoustic signal (into the frequency spectrum) around 20 % when pipe was surrounded by soil when compared with uncovered condition. However, the amplitude was enough to be detected clearly.

## **CHAPTER 5**

### **A SEMI AUTOMATED AIR COUPLED INVESTIGATION OF CONCRETE PIPE**

#### **5.1 Introduction**

This chapter involves the development of a semi- automated system that is intended to facilitate the quick completion of ACIE measurements. This development aims to build a more compact system to implement acoustic measurements and improve the speed of data collection. Applying the steel ball to excite P-wave is slow. Also, the typical condenser microphone is large. Thus, a solenoid impactor and micro electromechanical systems (MEMS) microphone investigated ACIE. The results obtained using condenser and MEMS microphone are compared.

##### **5.1.1 Semi-automated ACIE setup**

The circuit design for the semi-automated setup is illustrated in Figure 5-1. To excite the pipe, a push-pull style open frame solenoid electromagnet is utilized. It is rated at 12V with 8 mm stroke and is capable of generating 6 N force. A pulse generator (Wavetek model 166) is utilized to generate an input signal for the impactor. Then signal is then amplified using an audio power amplifier (MX-M542).



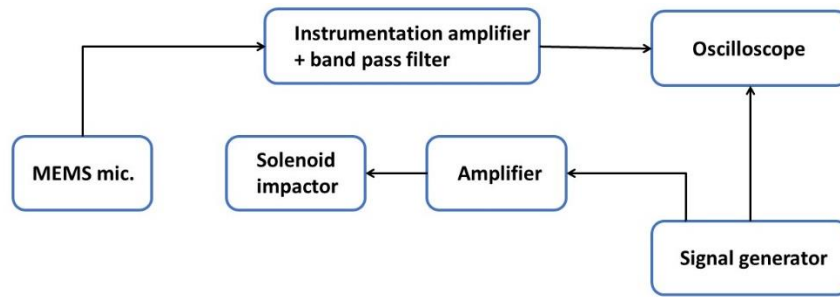


Figure 5-1: Block diagram of the circuit.

A broadband MEMS microphone with a band width of up to 80 kHz is used to record the acoustic signal. The microphone is connected to an instrumentation amplifier and band pass filter (2 kHz – 60 kHz). The data recorded by the oscilloscope is transferred to a computer and processed.

#### 5.1.2 Input waveform

Figure 5-2 depicts the input waveform used for excitation. A solenoid impactor can be excited using a variety of input waveforms generated by a signal generator. A square waveform has been used to excite the impactor [59]. However, there is a trade-off between the pulse width and the amplitude. The duration of the pulse determines the maximum frequency content generated and amplitude controls the level of impact force applied on the pipe. (It is important to determine the best pulse width and amplitude for the input waveform because using a very short pulse width will increase frequency content of pulse and the solenoid impactor may not be able to move quickly enough). After experimentation it was found that the pulse width of 2 ms with 1 V amplitude is optimal for this application.

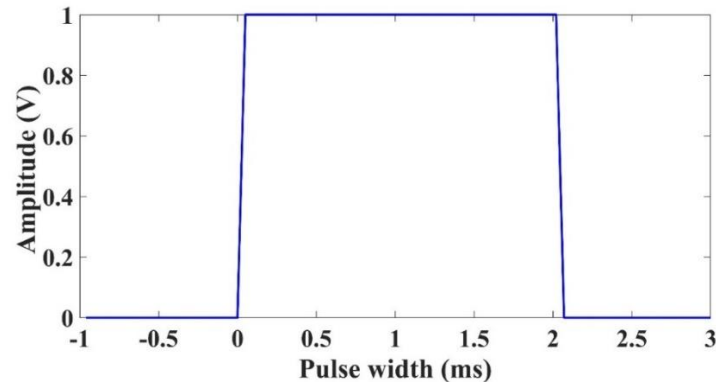


Figure 5-2: The input waveform for excitation.

### 5.1.3 Experimental setup

The schematic of the experimental setup has been shown in Figure 5-3.

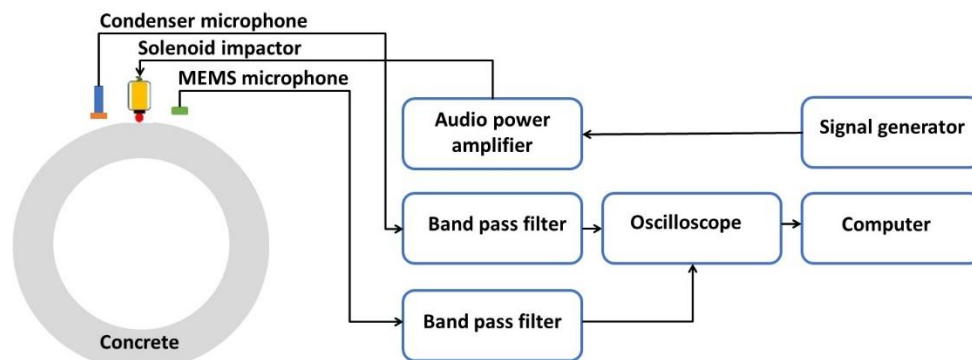


Figure 5-3: Schematic of experimental setup.

The setup using the condenser and MEMS microphone is depicted in Figure 5-4a. Figure 5-4d. depicts the push and pull type solenoid impactor that was utilized to provide the consistent point impact. A manual positioning system is used to move the impact hammer and sensor together along the surface of pipe. This study uses the same data acquisition as used in previous study.

(Chapter 4). The received signals are pre- processed using Hanning window and frequency spectrum is calculated using FFT function.

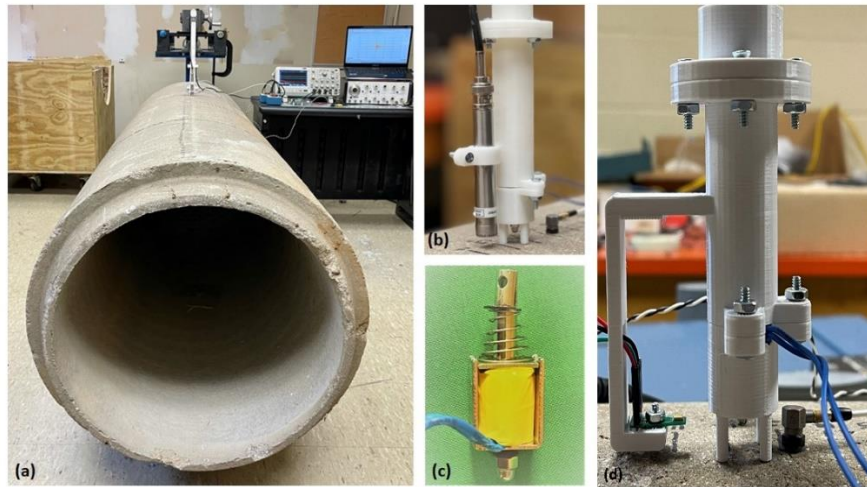


Figure 5-4: Photograph of the (a) experimental setup (b) Close-up showing microphone, accelerometer, and solenoid impactor (c) solenoid impactor (d) Impactor and MEMS microphone.

#### 5.1.4 Comparison between condenser and MEMS microphone

Figure 5-5 displays a comparison of the test outcomes for condenser and MEMS microphones. It was observed that the solenoid impactor is much noisier than the one generated by steel ball. This may be due to multiple reasons like influence of impactor and acoustic wave reflection created by the holder. Despite this, the thickness frequency peak is distinctly visible in frequency spectrum at 27.2 kHz.

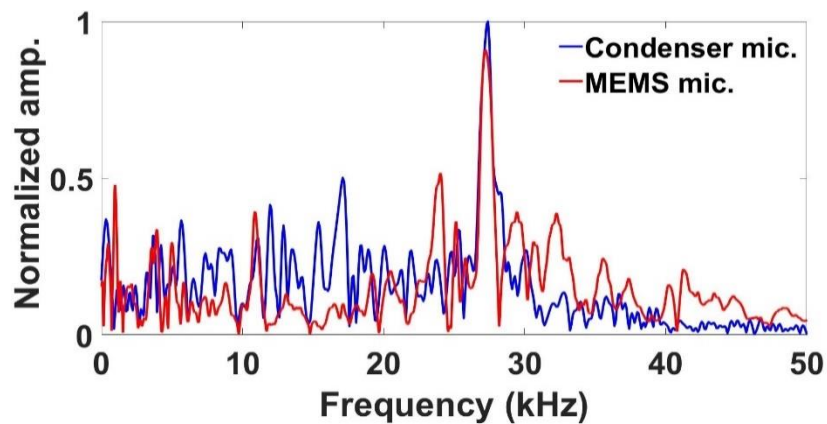


Figure 5-5: Frequency spectrum obtained using condenser and MEMS mic.

Using the acquired thickness frequency from frequency spectrum and P- wave velocity of the pipe obtained in the previous studies, the thickness of the pipe was 0.075 m which is very close to the actual value (0.076 m). This shows that both microphones provide signals of almost similar quality. Also, in conjunction with the use of a solenoid impactor, makes the setup more ideal for the ACIE technique by providing a constant and consistent impact.

## **5.2 Noise reduction study**

In prior study, it is demonstrated that MEMS microphones can receive leaky acoustic waves. But the signal is cluttered with higher levels of noise. As a result, in order to get rid of this a band pass filter is designed. There are several types of bandpass filter like Butterworth, Chebyshev, Bessel filter etc [61]. Figure 5-6a shows the frequency spectrum of raw data received from the microphone and filtered.

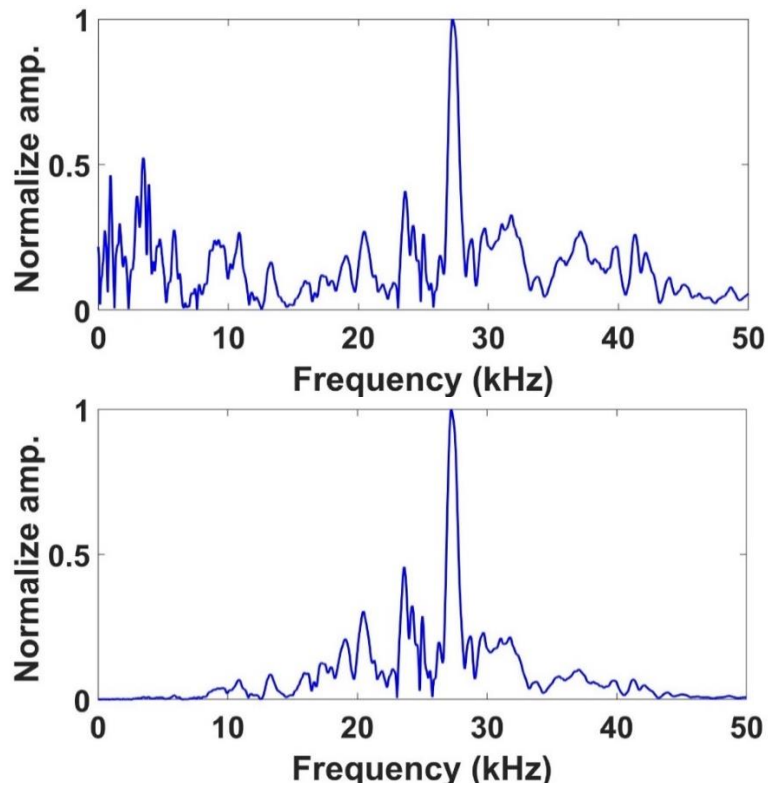


Figure 5-6: Frequency spectrum obtained using MEMS microphone's (a) Raw data (b) Filtered data.

Here, a Butterworth band pass filter has been utilized on the time response history. This filter is characterized by a flat frequency response in the passband [59]. The cutoff frequency between 15 kHz to 40 kHz has been set for filtering the received time response history and later FFT function was applied to obtain frequency spectra. It is clearly visible that the multiple frequency peaks other than thickness frequency are reduced frequency spectrum from filtered data.

### 5.3 Conclusions

Study findings lead to the following conclusions:

- It was observed that the MEMS microphone is capable of receiving the leaky acoustic waves generated and results are comparable to condenser microphone. Both microphones provide a thickness frequency at 27.2 kHz, but the signal is

noisier.

- The designed bandpass filter works effectively and reduces the unwanted frequency peaks from the spectrum other than the thickness frequency peak.

## CHAPTER 6

### INVESTIGATION OF PIPEWALL DEFECTS USING ACIE

#### 6.1 Introduction

Reinforced concrete pipes are commonly used in sewage and water supply due to corrosion-resistant and durability. In the United States, there are an estimated 860,000 miles of buried pipes supplying sewage and water to homes and businesses [62]. Approximately 40% of pipes are made of reinforced concrete, and an estimated 20-25% pipes show evidence of damage or defects. The deterioration and loss of strength in concrete pipelines is caused by a variety of factors like delamination, fractures, and voids of varying sizes. This chapter investigates if ACIE can be used to detect some of the flaws. The investigation is conducted by numerical simulation.

#### 6.2 Common flaws in concrete pipe.

There are several types of flaws which can appear in a concrete pipe and some of them are mentioned below:

##### 6.2.1 Thickness loss

Thickness loss, occurs when the concrete's surface is damaged and the concrete peels or flakes away, revealing the reinforcing steel underneath. This can be caused by several reasons, including freeze-thaw cycles, salt exposure etc. The corrosion of reinforcing steel in concrete can cause surface cracking and peeling, while sulfuric acid

reacting with cement can lead to thickness loss in the upper part of concrete pipes [59], [63] as shown in Figure 6-1.



Figure 6-1: Thickness loss due to corrosion [63].

### 6.2.2 Delamination

Concrete delamination is one of the most difficult challenges in concrete because of its unpredictable appearance and inconsistent pattern. The term "delamination" refers to the process by which concrete separates from the layer that serves as its foundation. Most common cause of cracks and delamination in reinforced concrete structures is corrosion of the rebars that hold the concrete together which contributes to decrease in the structure integrity [64]. A case of delamination in concrete structure is shown in Figure 6-2 [65] .





Figure 6-2: Delamination of concrete deck slab.

### 6.2.3 Soil voids

Wastewater can intrude into the surrounding soil due to pipe cracks, which can wash away the soil and create void. It is critical condition as it can significantly affect the pipe service life.

## 6.3 Numerical modeling of pipe wall defects

Three types of flaws in concrete pipe are investigated i.e., thickness loss (model 1), delamination (model 2) and fluid filled void (model 3). Figure 6-3 shows the schematic numerical model of flaws.

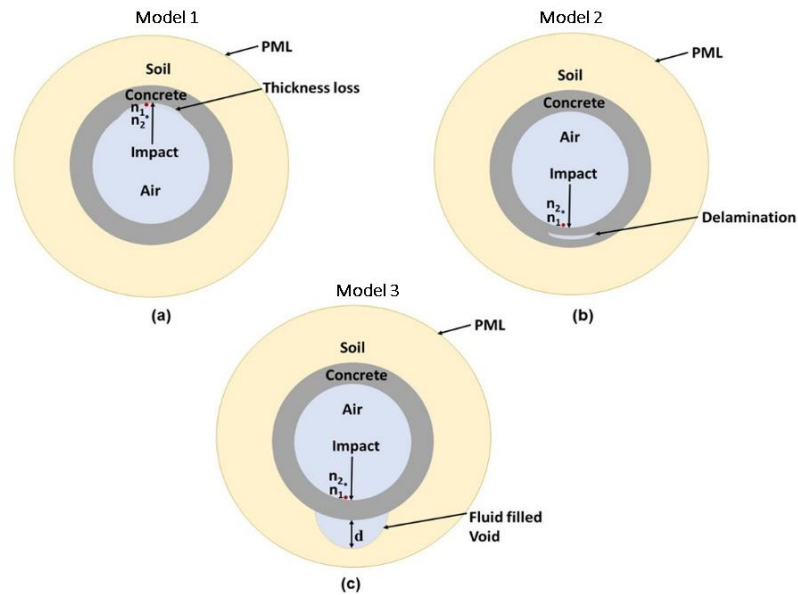


Figure 6-3: Illustration of flaws (a) thickness loss (b) delamination (c) Fluid filled void.

Model 1 with thickness loss is developed at the crown of the pipe due to corrosion. The actual dimension of the RCP is considered according to ASTM- C 76, having a type B- wall (thickness = 0.0762 m). To investigate the defect of thickness loss, the wall has been reduced by 0.012 m.

Model 2 represents delamination defects developed with dimension of 0.25 m by 0.05 m, positioned 0.05 m below the invert. Both model 1 and model 2 are simulated under non-buried and buried conditions.

Model 3 represents the fluid-filled void around the pipe located at concrete-soil interface. The voids are tested in three different sizes, with  $d_1 = 0.05$  m,  $d_2 = 0.12$  m and  $d_3 = 0.20$  m.

To simplify the analysis, concrete and soil are modeled as linear elastic isotropic material with properties as specified in Table 6-1.

Table 6-1: Elastic properties of concrete and soil [35], [56].

<b>Material</b>	Density (kg/m <sup>3</sup> )	Young's modulus (MPa)	Poisson's ratio
<b>Concrete</b>	2300	33100	0.2
<b>Soil</b>	2000	300	0.2

The outer boundary of soil is terminated by the PML boundary condition. A high-frequency Ricker wavelet is injected perpendicularly at selected node in each model and signal for both elastic and acoustic domains are captured. Mesh size of 2 mm and 1 mm is used for acoustic and elastic domains, respectively. Simulations are run for 1000-time steps (2 microsec) with a total duration of 2 ms for all simulations. Signal from both domains is pre-processed using a Hanning window and down-sampled. Signal length of 1 ms is used to obtain the frequency spectrum.

## 6.4 Results and discussion

### 6.4.1 Model 1: Effect of thickness loss

The normalized frequency response of signal received for buried and non-buried condition for thickness loss flaw is shown in Figure 6-4. Frequency spectra for the signal received in acoustic and elastic domain depict a clear resonant frequency of 29.9 kHz for both conditions.

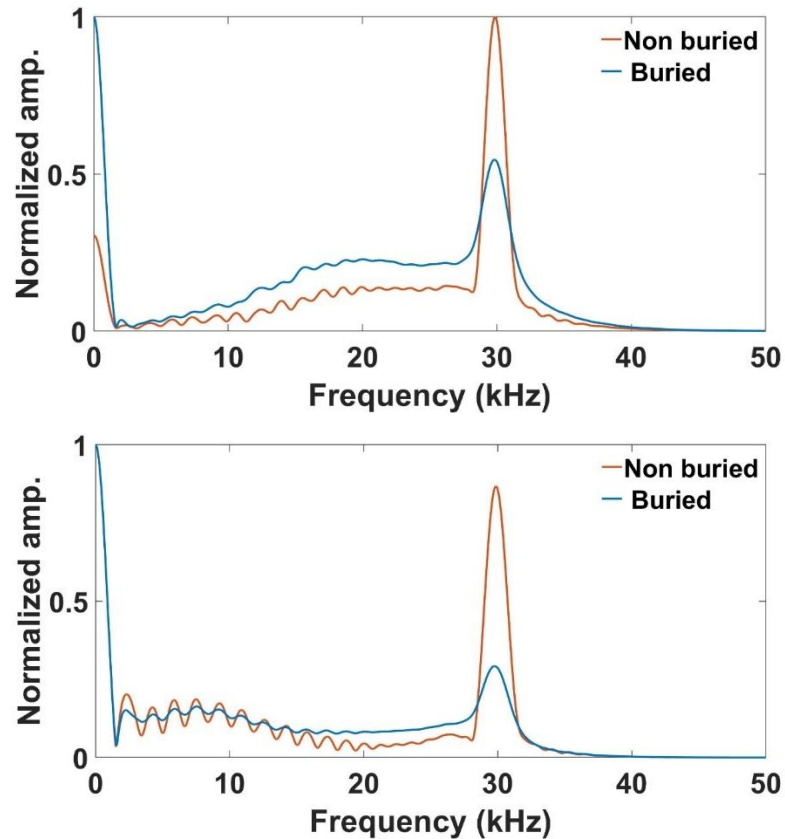


Figure 6-4: Frequency spectrum of thickness loss flaw for: a) acoustic domain b) elastic domain

For the buried condition, resonant frequency amplitude drops significantly in both domains, although it is visible at 29.9 kHz. The decrease in amplitude of the thickness frequency is due to acoustical impedance mismatch, as some amount of signal energy gets transferred to the soil. By using this thickness frequency and P-wave velocity of material in Eq. 2.1, the thickness of pipe is calculated as 0.064 m, which found close to the thickness considered in the model i.e., 0.063 m.

#### 6.4.2 Model 2: Effect of delamination

Next, the simulation of delamination in pipe is performed, and frequency response of signal received from both domains is shown in Figure 6-5.

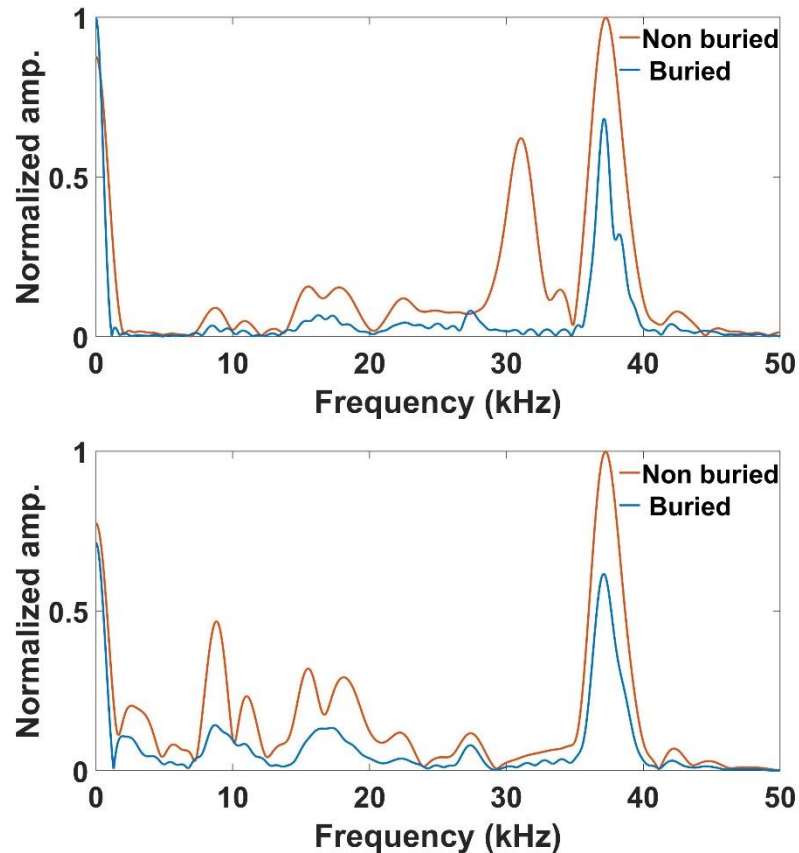


Figure 6-5: Frequency spectrum for delamination defect for a) acoustic domain b) elastic domain.

It has been observed that thickness frequency is located at 37.1 kHz for both domains. In this case, thickness frequency amplitude did not decrease significantly in either case. This is due to the fact that delamination creates a concrete/air interface in the pipe, and P- wave reflects approximately 100 % of wave energy at this interface. Moreover, the dominant frequency obtained from the model differed by less than 1 % from the theoretical value of 37.7 kHz. Using the dominant frequency and P-wave velocity in Equation 2.1, the delamination was calculated to be located at 0.05 m, which closely matches the true value of 0.051 m.

### 6.4.3 Model 3: Effect of soil void

Next, simulations result for three sized voids, ranging small to large, and frequency response of signal received from both domains are shown in Figure 6-6 (a & b). For comparison, results obtained from no void condition are also included.

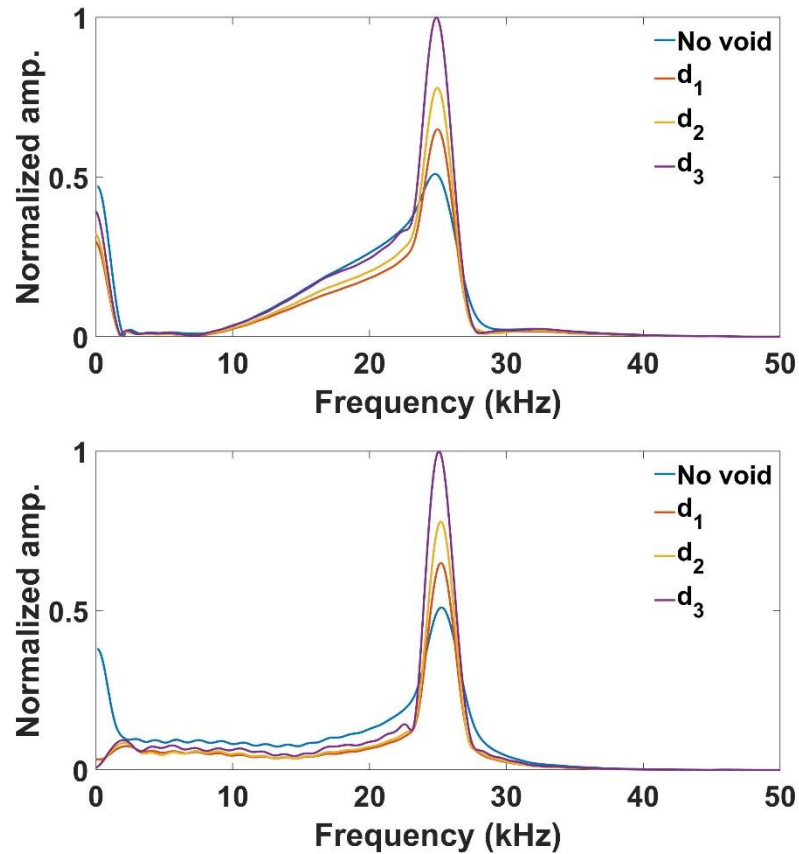


Figure 6-6: Influence of sizes of voids on thickness frequency response (a) Acoustic domain (b) Elastic domain.

As seen in Figure 6-6, thickness frequency is observed at 24.9 kHz in all cases for both domains. However, the amplitude of thickness frequency increased as the size of void increased. This is because when the concrete and soil are in full contact with each other at concrete-soil interface, the transfer of P- wave into the soil is significant. However, soil void will increase the concrete-air interface, and elastic waves will reflect

almost 100 %. As observed, the amplitude of thickness frequency increased substantially from no void to large void condition for the signal received from both domains.

## **6.5 Conclusions**

The numerical studies reported in this chapter were carried out to assess the feasibility of using ACIE to detect defects in concrete such as thickness loss and delamination, as well as voids ranging in size from small to big at the concrete/soil interface. The findings of this investigation are as follows:

- ACIE is able to detect common pipe wall defects in the buried condition. The results obtained from ACIE are compared to those from conventional IE technique and found to be reliable.

## **CHAPTER 7**

### **CONCLUSION**

This dissertation focused on investigation of buried reinforced concrete pipe using air coupled impact echo technique. To test its feasibility of ACIE technique first, a finite element analysis (FEA) based numerical simulation was conducted first. Both traditional IE and ACIE techniques were investigated using 2D and 3D models with acoustic - structure interaction in COMSOL Multiphysics software. Results obtained using ACIE was verified against IE. It was determined that the thickness frequency using a contact-based transducer could be estimated without contacting the pipe wall by capturing the acoustic wave that accompany the elastic wave resonance that occur in the IE process. Additionally, it is possible to capture the signal in a closed cavity, such as a concrete pipe (used in this research), without recording any acoustic wave reflections from the walls. Analysis has been done using a 2D as well as 3D. Both standalone and buried pipe were modelled. Two different types of soil were used around the pipe. As expected, the energy loss into the soil reduced the amount of the acoustic signal. However, the thickness frequency could still be determined.

After successful simulations, an experimental investigation was carried out in laboratory and ACIE technique was demonstrated using two commercially manufactured reinforced concrete pipe (RCP) samples were tested. The results acquired using the microphone match very well with the accelerometer data. A detailed parametric study was successfully carried



out to optimize the location of microphone and improved the signal reception.

A noise suppressor was developed to address the issue of direct acoustic noise as well as ambient noise. It has been discovered that this noise suppressor is able to significantly reduce signal noise and improve signal to noise ratio.

A semi-automated ACIE system was developed with the to speed up data collection. Traditionally the impact is applied manually with steel ball hammer. An electrically controlled solenoid impactor was utilized to excite the pipe automatically. Additionally, to make the system compact & cost effective, a MEMS microphone was employed to detect acoustic waves instead of a larger and more expensive condenser microphone. The results from both MEMS and the condenser microphones were comparable. However, significant noise was observed in the signal received by the MEMS microphone which was removed by a post-processing algorithm.

Finally, a numerical study was performed to test ACIE technique to detect common defects that occur a in concrete pipe. Three types of the defects were simulated: 1) thickness loss, 2) delamination and 3) soil void around the pipe. ACIE was able to detect all the defects successfully.

## **7.1 Future work**

In this work, ACIE for buried concrete pipe has been investigated. Even though the results of this research have been found to be satisfactory, there is still potential for development.

As a result, the following suggestions are made for consideration in future work:

- To accelerate the data collection and analysis a fully automated ACIE system for implementation within a pipe could be designed and tested.

- Conducting field study in realistic environment is recommended.
- Opportunity to develop more advanced signal processes should be explored.

## BIBLIOGRAPHY

- [1] J. M. Kang, S. Song, D. Park, and C. Choi, "Detection of cavities around concrete sewage pipelines using impact-echo method," *Tunn. Undergr. Space Technol.*, vol. 65, pp. 1–11, 2017.
- [2] M. Lehman, "The American Society of Civil Engineers' Report Card on America's Infrastructure," in *Women in Infrastructure*, P. Layne and J. S. Tietjen, Eds., in *Women in Engineering and Science*. Cham: Springer International Publishing, 2022, pp. 5–21. doi: 10.1007/978-3-030-92821-6\_2.
- [3] O. US EPA, "EPA's 6th Drinking Water Infrastructure Needs Survey and Assessment," Mar. 30, 2018. <https://www.epa.gov/dwsrf/epas-6th-drinking-water-infrastructure-needs-survey-and-assessment> (accessed Mar. 30, 2023).
- [4] F. Tosti and C. Ferrante, "Using Ground Penetrating Radar Methods to Investigate Reinforced Concrete Structures," *Surv. Geophys.*, vol. 41, no. 3, pp. 485–530, May 2020, doi: 10.1007/S10712-019-09565-5/METRICS.
- [5] A. du Plessis and W. P. Boshoff, "A review of X-ray computed tomography of concrete and asphalt construction materials," *Constr. Build. Mater.*, vol. 199, pp. 637–651, Feb. 2019, doi: 10.1016/J.CONBUILDMAT.2018.12.049.
- [6] T. Omar and M. L. Nehdi, "Remote sensing of concrete bridge decks using unmanned aerial vehicle infrared thermography," *Autom. Constr.*, vol. 83, pp. 360–371, 2017.
- [7] B. Mergelas and X. Kong, *Electromagnetic inspection of prestressed concrete pressure pipe*. American Water Works Association, 2001.
- [8] D.-S. Kim, W.-S. Seo, and K. M. Lee, "IE-SASW method for nondestructive evaluation of concrete structure," *NDT E Int.*, vol. 39, no. 2, pp. 143–154, 2006.
- [9] C.-P. Lin, C.-H. Lin, and C.-J. Chien, "Dispersion analysis of surface wave testing—SASW vs. MASW," *J. Appl. Geophys.*, vol. 143, pp. 223–230, 2017.
- [10] A. P. Jaganathan, "Multichannel surface wave analysis of reinforced concrete pipe segments using longitudinal and circumferential waves induced by a point impact," *J. Appl. Geophys.*, vol. 163, pp. 40–54, Apr. 2019, doi: 10.1016/J.JAPPGEO.2019.02.010.
- [11] Y. S. Cho, "Non-destructive testing of high strength concrete using spectral analysis of surface waves," *NDT E Int.*, vol. 36, no. 4, pp. 229–235, 2003.
- [12] H. Chen *et al.*, "Interfacial debonding detection for rectangular cfst using the masw method and its physical mechanism analysis at the meso-level," *mdpi.com*, 2019, doi: 10.3390/s19122778.

- [13] N. Ryden, C. B. Park, P. Ulriksen, and R. D. Miller, "Multimodal approach to seismic pavement testing," *J. Geotech. Geoenvironmental Eng.*, vol. 130, no. 6, pp. 636–645, 2004.
- [14] K. Gavin, W. Broere, M. S. Kovacevic, K. G. Gavin, W. Broere, and M. S. Kovačević, "Investigation of the remaining life of an immersed tube tunnel in The Netherlands," *taylorfrancis.com*, 2019, doi: 10.4324/9781003031666-23.
- [15] J. S. Popovics and O. Abraham, "Surface wave techniques for evaluation of concrete structures," *Non-Destr. Eval. Reinf. Concr. Struct. Non-Destr. Test. Methods*, pp. 441–465, 2010, doi: 10.1533/9781845699604.2.441.
- [16] J.-M. Lin and M. Sansalone, "The transverse elastic impact response of thick hollow cylinders," *J. Nondestruct. Eval.*, vol. 12, no. 2, pp. 139–149, 1993.
- [17] J. M. Lin and M. Sansalone, "Impact-echo response of hollow cylindrical concrete structures surrounded by soil and rock. Part 1. Numerical studies," *Geotech. Test. J.*, vol. 17, no. 2, pp. 207–219, 1994, doi: 10.1520/GTJ10092J.
- [18] C. R. Kommireddi and S. L. Gassman, "Impact echo evaluation of thin walled concrete pipes," *Proc. ASCE Pipeline Div. Spec. Congr. - Pipeline Eng. Constr.*, pp. 291–300, 2004, doi: 10.1061/40745(146)29.
- [19] B. O. J. Owino and L. J. Jacobs, "Attenuation Measurements in Cement-Based Materials Using Laser Ultrasonics," *J. Eng. Mech.*, vol. 125, no. 6, pp. 637–647, Jun. 1999, doi: 10.1061/(ASCE)0733-9399(1999)125:6(637).
- [20] J. Zhu and J. S. Popovics, "Imaging Concrete Structures Using Air-Coupled Impact-Echo," *J. Eng. Mech.*, vol. 133, no. 6, pp. 628–640, Jun. 2007, doi: 10.1061/(ASCE)0733-9399(2007)133:6(628).
- [21] J. Zhu, J. P.-A. C. Proceedings, and undefined 2002, "Non-contact detection of surface waves in concrete using an air-coupled sensor," *aip.scitation.org*, [Online]. Available: <https://aip.scitation.org/doi/abs/10.1063/1.1472940>
- [22] X. Dai, J. Zhu, Y.-T. Tsai, and M. R. Haberman, "Use of parabolic reflector to amplify in-air signals generated during impact-echo testing," *J. Acoust. Soc. Am.*, vol. 130, no. 4, pp. EL167–EL172, 2011.
- [23] F. Schubert, H. Wigggenhauser, and R. Lausch, "On the accuracy of thickness measurements in impact-echo testing of finite concrete specimens—numerical and experimental results," *Ultrasonics*, vol. 42, no. 1–9, pp. 897–901, 2004.
- [24] S.-H. Kee, T. Oh, J. S. Popovics, R. W. Arndt, and J. Zhu, "Nondestructive bridge deck testing with air-coupled impact-echo and infrared thermography," *J. Bridge Eng.*, vol. 17, no. 6, pp. 928–939, 2012.

- [25] T. Oh, S.-H. Kee, R. W. Arndt, J. S. Popovics, M. Asce, and J. Zhu, "Comparison of NDT methods for assessment of a concrete bridge deck," *ascelibrary.org*, vol. 139, no. 3, pp. 305–314, Mar. 2013, doi: 10.1061/(ASCE)EM.1943-7889.0000441.
- [26] R. Groschup and C. U. Grosse, "Development of an Efficient Air-Coupled Impact-Echo Scanner for Concrete Pavements," in *Proceedings of the World Conference on Non-Destructive Testing*, 2016.
- [27] L. D. Olson, Y. Tinkey, and P. Miller, "Concrete Bridge Condition Assessment with Impact Echo Scanning," pp. 59–66, Apr. 2012, doi: 10.1061/47629(408)8.
- [28] D. G. Aggelis, T. Shiotani, and K. Kasai, "Evaluation of grouting in tunnel lining using impact-echo," *Tunn. Undergr. Space Technol.*, vol. 23, no. 6, pp. 629–637, Nov. 2008, doi: 10.1016/j.tust.2007.12.001.
- [29] A. S. Zein, M. Asce, and S. L. Gassman, "Frequency Spectrum Analysis of Impact-Echo Waveforms for T-Beams," *J. Bridge Eng.*, vol. 15, no. 6, pp. 705–714, Nov. 2010, doi: 10.1061/(ASCE)BE.1943-5592.0000107.
- [30] F. Fetrat, *Application of seismic surface-waves in concrete bridge-deck evaluation*. Rutgers The State University of New Jersey-New Brunswick, 2016.
- [31] N. J. Carino and M. Sansalone, "Flaw Detection in Concrete Using the Impact-Echo Method," *Bridge Eval. Repair Rehabil.*, pp. 101–118, 1990, doi: 10.1007/978-94-009-2153-5\_8.
- [32] M. J. Sansalone and W. B. Streett, "IMPACT-ECHO. NONDESTRUCTIVE EVALUATION OF CONCRETE AND MASONRY," 1997, Accessed: Mar. 30, 2023. [Online]. Available: <https://trid.trb.org/view/573779>
- [33] N. J. Carino, "The impact-echo method: an overview," *Struct. 2001 Struct. Eng. Odyssey*, pp. 1–18, 2001.
- [34] F. Schubert, B. K.-J. of N. Evaluation, and undefined 2008, "Ten lectures on impact-echo," *Springer*, vol. 27, no. 1–3, pp. 5–21, 2016, doi: 10.1007/s10921-008-0036-2.
- [35] J. M. Lin, M. S.-G. testing journal, and undefined 1994, "Impact-echo response of hollow cylindrical concrete structures surrounded by soil and rock: part II—experimental studies," *astm.org*, [Online]. Available: [https://www.astm.org/DIGITAL\\_LIBRARY/JOURNALS/GEOTECH/PAGES/GTJ10093J.htm](https://www.astm.org/DIGITAL_LIBRARY/JOURNALS/GEOTECH/PAGES/GTJ10093J.htm)
- [36] R. Groschup and C. U. Grosse, "MEMS Microphone Array Sensor for Air-Coupled Impact-Echo," *Sens. 2015 Vol 15 Pages 14932-14945*, vol. 15, no. 7, pp. 14932–14945, Jun. 2015, doi: 10.3390/S150714932.

- [37] M. R. Cho, H. S. Lee, H. H. Kim, and K. B. Kim, "Finite element analysis of the impact-echo testing at a concrete slab with complex boundary conditions," *KSCE J. Civ. Eng.*, vol. 9, no. 2, pp. 113–117, Mar. 2005, doi: 10.1007/BF02829064/METRICS.
- [38] J. Lu, "Advancements in evaluation of air-coupled impact-echo test method," Iowa State University, 2015.
- [39] P.-A. Wernberg, "Structure-Acoustic Analysis; Methods, Implementations and Applications," 2006.
- [40] M. H. Sadd, *Elasticity: theory, applications, and numerics*. 2009. [Online].
- [41] P. Davidsson, *Structure-acoustic analysis; finite element modelling and reduction methods*. 2004. [Online]. Available: <https://lup.lub.lu.se/record/467245>
- [42] C. Cheng and M. Sansalone, "The impact-echo response of concrete plates containing delaminations: numerical, experimental and field studies," *Mater. Struct.*, vol. 26, no. 5, pp. 274–285, Jun. 1993, doi: 10.1007/BF02472949/METRICS.
- [43] F. Dethof, D. Algernon, C. Thurnherr, and S. K.-A. sn oi ta cil pp, "How to conduct Impact Echo simulations for non-destructive testing at concrete structures for the nuclear industry," *aaltodoc.aalto.fi*, [Online]. Available: <https://aaltodoc.aalto.fi/bitstream/handle/123456789/119824/isbn9789526411408.pdf?sequence=1&isAllowed=y#page=125>
- [44] C. Hsiao, C. C. Cheng, T. Liou, Y. J.-N. & E. International, and undefined 2008, "Detecting flaws in concrete blocks using the impact-echo method," *Elsevier*, [Online]. Available: <https://www.sciencedirect.com/science/article/pii/S0963869507001065>
- [45] O. Baggens and N. Ryden, "Systematic errors in Impact-Echo thickness estimation due to near field effects," *NDT E Int.*, vol. 69, pp. 16–27, Jan. 2015, doi: 10.1016/J.NDTEINT.2014.09.003.
- [46] N. Ricker, "The form and laws of propagation of seismic wavelets," *Geophysics*, vol. 18, no. 1, pp. 10–40, Jan. 1953, doi: 10.1190/1.1437843.
- [47] A. G. Salehabady, "Why Ricker Wavelets Are Successful In Processing Seismic Data: Towards A Theoretical Explanation," 2014.
- [48] Y. Wang, "Frequencies of the Ricker wavelet," *Httpsdoiorg101190geo2014-04411*, vol. 80, no. 2, pp. A31–A37, Feb. 2015, doi: 10.1190/GEO2014-0441.1.
- [49] P. L. Yeh and P. L. Liu, "Application of the wavelet transform and the enhanced Fourier spectrum in the impact echo test," *NDT E Int.*, vol. 41, no. 5, pp. 382–394, Jul. 2008, doi: 10.1016/J.NDTEINT.2008.01.002.

- [50] F. Moser, L. J. Jacobs, and J. Qu, “Modeling elastic wave propagation in waveguides with the finite element method,” *Ndt E Int.*, vol. 32, no. 4, pp. 225–234, 1999.
- [51] M. N. Ichchou, S. Akrouf, and J.-M. Mencik, “Guided waves group and energy velocities via finite elements,” *J. Sound Vib.*, vol. 305, no. 4–5, pp. 931–944, 2007.
- [52] D. Alleyne and P. Cawley, “A two-dimensional Fourier transform method for the measurement of propagating multimode signals,” *J. Acoust. Soc. Am.*, vol. 89, no. 3, pp. 1159–1168, 1991.
- [53] “Standard Specification for Reinforced Concrete Culvert, Storm Drain, and Sewer Pipe.” <https://www.astm.org/c0076-22.html> (accessed Mar. 30, 2023).
- [54] M. Sansalone, “Impact-echo: The complete story,” *Struct. J.*, vol. 94, no. 6, pp. 777–786, 1997.
- [55] A. C. P. Association, *Concrete pipe and box culvert installation*. 2007. [Online]. Available: <https://books.google.com/books?hl=en&lr=&id=nKSTjRwpqEMC&oi=fnd&pg=PT4>
- [56] A. P. Jaganathan, “Experimental implementation of multichannel surface wave analysis of a concrete pipe along lengthwise direction,” *J. Appl. Geophys.*, vol. 180, p. 104132, Sep. 2020, doi: 10.1016/J.JAPPGEO.2020.104132.
- [57] J. Tcherter, L. Olson, D. Sack, and P. Miller, “Non-destructive evaluation techniques for evaluation of nuclear concrete structures with limited accessibility”.
- [58] K. Chen, Z. Zhang, and Y. Zhou, “Application of surface wave in reinforced concrete invert detection,” *IOP Conf. Ser. Earth Environ. Sci.*, vol. 660, no. 1, p. 012069, Feb. 2021, doi: 10.1088/1755-1315/660/1/012069.
- [59] A. V. Oppenheim, A. S. Willsky, S. Hamid, and J.-J. Ding, *Signals and systems*. 1997. [Online]. Available: [https://teacher.yuntech.edu.tw/~htchang/CH2\\_nv.pdf](https://teacher.yuntech.edu.tw/~htchang/CH2_nv.pdf)
- [60] J. F. Scherr and C. U. Grosse, “Delamination detection on a concrete bridge deck using impact echo scanning,” *Struct. Concr.*, vol. 22, no. 2, pp. 806–812, Apr. 2021, doi: 10.1002/SUCO.202000415.
- [61] J. V. Calvano, V. C. Alves, and M. Lubaszewski, “Fault detection methodology and BIST method for 2nd order Butterworth, Chebyshev and Bessel filter approximations,” in *Proceedings 18th IEEE VLSI Test Symposium*, Apr. 2000, pp. 319–324. doi: 10.1109/VTEST.2000.843861.
- [62] “Water Main Break Rates In the USA and Canada: A Comprehensive Study,” 2018.

- [63] H. Fang *et al.*, “Experimental and numerical study on mechanical analysis of buried corroded concrete pipes under static traffic loads,” *mdpi.com*, doi: 10.3390/app9235002.
- [64] C. Q. Li, J. J. Zheng, W. Lawanwisut, and R. E. Melchers, “Concrete Delamination Caused by Steel Reinforcement Corrosion,” *J. Mater. Civ. Eng.*, vol. 19, no. 7, pp. 591–600, Jul. 2007, doi: 10.1061/(ASCE)0899-1561(2007)19:7(591).
- [65] “NDT/Diagnostic Tools Archives,” *Vertical Access*, Jan. 15, 2020. <https://vertical-access.com/category/ndtdiagnostic-tools/> (accessed Mar. 30, 2023).